



HAL
open science

Förster Resonance Energy Transfer Based Biosensor for Targeting the hNTH1–YB1 Interface as a Potential Anticancer Drug Target

Muge Senarisoy, Caroline Barette, Françoise Lacroix, Salvatore Debonis, Meike Stelter, Fabienne Hans, Jean-Philippe Kleman, Marie-Odile Fauvarque, Joanna Timmins

► To cite this version:

Muge Senarisoy, Caroline Barette, Françoise Lacroix, Salvatore Debonis, Meike Stelter, et al.. Förster Resonance Energy Transfer Based Biosensor for Targeting the hNTH1–YB1 Interface as a Potential Anticancer Drug Target. *ACS Chemical Biology*, 2020, 15 (4), pp.990-1003. 10.1021/acscchembio.9b01023 . cea-02517754

HAL Id: cea-02517754

<https://cea.hal.science/cea-02517754>

Submitted on 23 Nov 2020

HAL is a multi-disciplinary open access archive for the deposit and dissemination of scientific research documents, whether they are published or not. The documents may come from teaching and research institutions in France or abroad, or from public or private research centers.

L'archive ouverte pluridisciplinaire **HAL**, est destinée au dépôt et à la diffusion de documents scientifiques de niveau recherche, publiés ou non, émanant des établissements d'enseignement et de recherche français ou étrangers, des laboratoires publics ou privés.

A FRET-based biosensor for targeting the hNTH1-YB1 interface as a potential anti-cancer drug target

Muge Senarisoy¹, Caroline Barette², Françoise Lacroix¹, Salvatore De Bonis¹, Meike Stelter¹, Fabienne Hans¹, Jean-Philippe Kleman¹, Marie-Odile Fauvarque² and Joanna Timmins^{1*}.

¹Univ. Grenoble Alpes, CEA, CNRS, IBS, F-38000 Grenoble, France.

²Univ. Grenoble Alpes, CEA, INSERM, BGE, F-38000 Grenoble, France.

*Corresponding author: Joanna Timmins (Joanna.timmins@ibs.fr)

Abstract

The Y-box binding protein 1 (YB1) is an established metastatic marker: high expression and nuclear localization of YB1 correlate with tumor aggressiveness, drug resistance and poor patient survival in various tumors. In the nucleus, YB1 interacts with and regulates the activities of several nuclear proteins, including the DNA glycosylase, human Endonuclease III (hNTH1). In the present study, we used Förster Resonance Energy Transfer (FRET) and AlphaLISA technologies to further characterize this interaction and define the minimal regions of hNTH1 and YB1 required for complex formation. This work led us to design an original and cost-effective FRET-based biosensor for the rapid *in vitro* high-throughput screening for potential inhibitors of the hNTH1-YB1 complex. Two pilot screens were carried out allowing the selection of several promising compounds exhibiting IC₅₀ values in the low micromolar range. Interestingly, two of these compounds bind to YB1 and sensitize drug-resistant breast tumor cells to the chemotherapeutic agent, cisplatin. Taken together, these findings demonstrate that the hNTH1-YB1 interface is a druggable target for the development of new therapeutic strategies for the treatment of drug-resistant tumors. Moreover, beyond this study, the simple design of our biosensor defines an innovative and efficient strategy for the screening of inhibitors of therapeutically relevant protein-protein interfaces.

INTRODUCTION

The most common non-surgical cancer treatments function by generating DNA damage either directly or indirectly. Damage to DNA induces several cellular responses that enable the cell either to eliminate or cope with the damage, or activate a programmed cell death process, presumably to eliminate cells with potentially catastrophic mutations.¹ In mammals, several DNA repair pathways are responsible for removal of DNA lesions and thus ensure genomic stability.² Deficiencies in any of these pathways may accelerate the process of carcinogenesis³ and conversely, enhanced DNA repair pathways provide a resistance mechanism to initially effective cytotoxic therapies.¹ Radiotherapy and several chemotherapeutic drugs induce oxidative stress in exposed tumor cells. The base excision repair (BER) pathway is responsible for the removal of small base lesions resulting from deamination, oxidation, or methylation;^{4,5} its efficiency can thus reduce the cytotoxic effects of certain anticancer drugs. As a result, the proteins involved in BER are increasingly considered as targets for cancer treatment.⁶⁻⁸

Human NTH1 (eNdonuclease THree) is a bifunctional DNA glycosylase (possessing both DNA glycosylase and apurinic or apyrimidic (AP) lyase activities; Figure 1), responsible for the removal of oxidized pyrimidines.⁹ hNTH1's catalytic activity is tightly regulated.¹⁰ Its N-terminal mammalian-specific domain (NTD), which is predicted to be largely disordered, plays an auto-inhibitory role, which most likely explains its reduced activity compared to that of its *E. coli* homologue.¹¹ Dimerization of hNTH1 occurring via NTD interactions actually disrupts the inhibitory effect of the NTD.¹⁰ hNTH1 also has several interaction partners, which regulate its enzymatic reaction. The nucleotide excision repair (NER) enzyme, XPG, binds directly to hNTH1 and enhances its binding to damaged DNA (Figure 1).^{12,13} Moreover, the AP-endonuclease, APE1, is known to stimulate hNTH1's glycosylase activity against thymine glycol (oxidized form of thymine) paired with adenine.¹⁴ Finally, a direct interaction between hNTH1 and the multifunctional Y-box binding protein 1 (YB1) has been reported and was shown to enhance the AP-lyase activity of hNTH1 (Figure 1).¹⁵

Interestingly, YB1 is also an established metastatic marker, and high expression of YB1 correlates with tumor aggressiveness and poor patient survival in diverse tumor types.¹⁶⁻¹⁹ Many reports have also shown a possible link between YB1 and drug resistance both in cell cultures and in clinical human tumor samples. For example, the cellular localization and expression levels of YB1 correlate with cellular sensitivities to the cytotoxic effects of cisplatin and other DNA-damaging agents.²⁰ Several studies have indeed demonstrated that the level of nuclear expression of YB1 is predictive of drug resistance and poor prognosis in breast tumors, ovarian cancers and synovial sarcomas.²¹⁻²⁶ The

nucleo-cytoplasmic distribution of YB1 is regulated by a non-canonical nuclear localization signal (NLS) and a cytoplasmic retention site (located in the C-terminal region of YB1), which prevails over the NLS and therefore confers a mainly cytoplasmic localization to YB1.^{17,27} However, in response to environmental stress, including exposure to genotoxic agents, the 20S proteasome cleaves YB1, and a C-terminally truncated form of YB1 (YB1 Δ C), corresponding to residues 1-219, is translocated to the nucleus.²⁸

In the nucleus, YB1 becomes involved in transcription regulation, DNA repair and replication, and pre-mRNA splicing.²⁷ YB1 has been shown to interact with and regulate the activities of several nuclear proteins, such as the topoisomerase I,²⁹ and several DNA repair proteins, including hNTH1.¹⁵ In the MCF7 breast adenocarcinoma cell line, Guay and co-workers observed an increase in hNTH1-YB1 complex formation after exposure to UV light or the chemotherapeutic agent, cisplatin, but not to other DNA damaging agents, such as camptothecin and mitomycin C.³⁰ Both UV light and cisplatin are known to cause oxidative stress and lead to the formation of oxidized bases. Moreover, in this same study the authors also reported that knocking down hNTH1 protein levels sensitized cells to both UV light and cisplatin – a very similar effect to that observed when knocking-down YB1.³⁰ Together these findings suggest that YB1 acts in concert with hNTH1 in the response of MCF7 cells to cisplatin and indicate that the hNTH1-YB1 interface may be a valid target for the development of new anticancer drugs for the treatment of cisplatin-resistant tumors.

In the present study, we have further characterized the interaction between hNTH1 and YB1 *in vitro* and *in cellulo* to define the domains involved in this interaction. This led us to design and optimize a very robust Förster Resonance Energy Transfer (FRET) based biosensor for the *in vitro* screening of chemical libraries in order to identify potential inhibitors of the hNTH1-YB1 complex. Two pilot screens were carried out using this biosensor and allowed the selection of several compounds exhibiting IC₅₀ values in the low micromolar range, which were further validated *in vitro* using an orthogonal assay. Of these, two compounds bind to YB1 and partially restore sensitivity of MCF7 cells to cisplatin, thereby demonstrating that the hNTH1-YB1 interface is a druggable target for the development of new anticancer agents and that our biosensor represents a highly efficient and low-cost tool for the screening of chemical libraries for the identification of inhibitors of protein-protein interactions (PPI).

RESULTS AND DISCUSSION

YB1 stimulates the AP-lyase activity of hNTH1

Using purified hNTH1 and YB1 proteins, we measured the rates of DNA glycosylase and AP-lyase activities of hNTH1 on a 35mer dsDNA substrate containing thymine glycol paired with adenine

in the absence and presence of an excess of wild-type YB1 (Figure 2A). As reported previously, YB1 did not affect the DNA glycosylase activity of hNTH1, but instead was found to specifically stimulate the rate of AP lyase activity of hNTH1 (Figures 1 and 2A, and Supplementary Figure 1) in agreement with earlier data.¹⁵ Indeed, in the absence of YB1, we observed a clear uncoupling of hNTH1's activities on such a substrate with a glycosylase rate significantly faster than the AP-lyase activity, as reported previously.^{14,15,31,32} Upon addition of YB1, however, after the initial lag phase due to the lack of AP-lyase substrate (0-5 min), the steady-state rate of the AP-lyase activity was increased to a level similar to that measured for the DNA glycosylase activity alone (see table in Figure 2A). Through its interaction with hNTH1, YB1 thus appears to favor the coupling of hNTH1's bifunctional activities.

We then performed interaction studies using AlphaLISA technology to identify the regions of hNTH1 and YB1 involved in this specific interaction. For this, His-tagged hNTH1 was bound to Anti-His coated acceptor beads and biotinylated YB1 was bound to streptavidin-coated donor beads. We performed various titration experiments using different combinations of hNTH1 and YB1 constructs and the results presented in Figure 2B indicate that the NTD of hNTH1, which is known to play a key role in regulating hNTH1's catalytic activity,¹¹ is critical and sufficient for interaction with YB1. In contrast, the C-terminal region of YB1, which is missing in the nuclear form of YB1 (*i.e.* YB1 Δ C), is dispensable for this interaction. To estimate the binding affinity of the hNTH1-YB1 Δ C complex, we additionally performed a competition assay in which increasing amounts of untagged hNTH1 was titrated into an AlphaLISA reaction containing biotinylated YB1 Δ C and His-tagged hNTH1 (Figure 2C). The IC₅₀ derived from this data provides an estimate of the binding affinity of the hNTH1-YB1 Δ C complex and was found to be $0.4 \pm 0.2 \mu\text{M}$.

hNTH1-YB1 interaction *in vitro* and *in cellulo*

To validate these findings, we decided to evaluate the interaction between hNTH1 and YB1 Δ C using FRET measurements, which can be applied both *in vitro* and *in cellulo*. For the *in vitro* studies, we expressed and purified different forms of hNTH1 and YB1 Δ C coupled to mTurquoise2 (mTQ2) and super yellow fluorescent protein 2 (SYFP2), respectively. These two fluorescent proteins are two of the brightest fluorescent proteins suitable for FRET experiments.^{33,34} We mixed SYFP2-YB1 Δ C or YB1 Δ C-SYFP2 with either mTQ2 alone, mTQ2-hNTH1 or hNTH1-mTQ2 and measured the FRET efficiencies of these mixes (Figure 3A). As expected, the mixtures with mTQ2 alone did not show any FRET signal (<0.5%). In contrast, both mTQ2-hNTH1 and hNTH1-mTQ2 containing mixes produced significant FRET levels, thereby confirming that YB1 Δ C efficiently interacts with hNTH1. We noticed, however, that the FRET efficiency was significantly influenced by the position of the fluorescent proteins: the highest FRET efficiency was obtained when the fluorescent proteins were fused to the C-termini of both hNTH1

and YB1 Δ C constructs. Indeed, in the presence of YB1 Δ C-SYFP2, the hNTH1-mTQ2 construct produced a FRET signal three times higher than that obtained with mTQ2-hNTH1.

To investigate the interaction between hNTH1 and YB1 in cells, we prepared a stably transfected MCF7 cell line expressing hNTH1-mTQ2 and transiently transfected this cell line with either SYFP2-NLS (nuclear localized form of SYFP2 used as a negative control), YB1 Δ C-SYFP2 or SYFP2- YB1 Δ C containing plasmids (Figure 3B-E). *In cellulo* FRET measurements using the acceptor photobleaching method were carried out on MCF7 cells displaying co-expression of hNTH1-mTQ2 and SYFP2 constructs in the nucleus. Because the transfection efficiency was low, such cells were rare (<1%). The expression levels of YB1 Δ C constructs were also variable from cell to cell, with most of the cells showing intense SYFP2 signals. The gradual acceptor photobleaching experiments were performed on such cells, which clearly also exhibited the highest FRET levels. The mean FRET efficiencies measured on MCF7 cells stably transfected with hNTH1-mTQ2 and transiently expressing SYFP2-NLS, YB1 Δ C-SYFP2 or SYFP2-YB1 Δ C were of 1.3, 15.4 and 22.0% respectively (Figure 3E). The strongest FRET signal was obtained from stably transfected MCF7 cells transiently expressing YB1 Δ C-SYFP2 (Figure 3D). Thus, as with our *in vitro* measurements, a configuration in which both mTQ2 and SYFP2 are fused to the C-termini of hNTH1 and YB1 Δ C resulted in the strongest FRET levels. In this configuration, the FRET efficiency was significantly higher than that of the negative control clearly indicating that hNTH1 and YB1 Δ C interact in the nuclei of MCF7 cells.

The levels of nuclear YB1 have been shown to be largely increased in cells exposed to genotoxic stress and high levels of YB1 are predictive of drug resistance and poor prognosis.²¹⁻²⁶ Interestingly, we observe strong FRET signal in the absence of exposure to anticancer agents, but only in cells overexpressing high levels of YB1 Δ C. Taken together, these findings suggest that the increased abundance of nuclear YB1, resulting from cleavage and translocation of YB1 to the nucleus in response to genotoxic stress, favors its interaction with hNTH1 and the stimulation of its DNA repair activity. In turn, this enhanced DNA repair activity may contribute to the development of drug resistance. Interfering with the hNTH1-YB1 interaction could thus provide clinicians with a new therapeutic strategy for the treatment of drug resistant solid tumors.

Design of a FRET-based biosensor

Targeting PPIs for drug development is attracting increasing attention,³⁵ but discovering small-molecules that disrupt PPIs is very challenging. Several databases and chemical libraries have been developed in order to facilitate the search for potential inhibitors^{36,37} and various experimental approaches are used to identify initial lead compounds even in the absence of high-resolution structural information. The most common assays rely on either AlphaScreen (and its related AlphaLISA

assay), time-resolved FRET (TR-FRET), or time-resolved fluorescence (TRF) assays, all of which have both advantages and disadvantages.³⁸ Here we used the highly sensitive AlphaLISA assay to study the *in vitro* interaction of hNTH1 with YB1 and determine the apparent affinity of the complex. However, the major limitations of this assay for high throughput screening (HTS) resides in its cost and the sensitivity of the beads to ambient light, which causes high variability in the measurements and reduces storage time.

The success of our FRET measurements prompted us to design a cost-effective FRET-based biosensor adapted to HTS technology for the selection of potential inhibitors of the hNTH1-YB1 complex. FRET-based HTS assays relying on the use of genetically encoded fluorescent proteins are mostly performed by mixing donor- and acceptor-labelled protein partners.³⁹⁻⁴¹ In contrast, the basic design of this biosensor consisted of a single fusion polypeptide chain encoding both the fluorescent tags and the target proteins with 5-10 amino acid linkers in between each protein (Figure 4A), similar in design to previously reported constructs of FRET-based biosensors.⁴² Based on our *in vitro* and *in cellulo* FRET data, SYFP2 was placed at the amino-terminus and mTQ2 at the C-terminus of the construct, while the YB1 Δ C and hNTH1 proteins were inserted in between forming a fusion protein composed of SYFP2-YB1 Δ C-hNTH1-mTQ2, which from hereon we will refer to as Biosensor 1. This large (116kDa) protein chain was overexpressed in *E. coli* and purified for *in vitro* FRET measurements. Protein purity was critical for our assays, since DNA or protein (and particularly fluorescent protein) contamination would interfere with subsequent fluorescence measurements and calculations of FRET efficiencies in which we assume to have a 1:1 ratio of mTQ2 and SYFP2 in our samples. In the case of Biosensor 1, the protein yield was high (2 mg L⁻¹ culture) and less than 10 mg of protein were sufficient to perform the screens described below.

Having both protein partners within a single polypeptide chain greatly simplifies the protein-protein interaction assay by reducing the number of samples to purify and ensuring a strict 1:1 molar ratio of the two components. As controls, several alternative biosensor constructs were prepared (Figure 4B) missing either one of the two target proteins (SYFP2-YB1 Δ C-mTQ2, corresponding to Biosensor 2, and SYFP2-hNTH1-mTQ2, corresponding to Biosensor 3) or inverted (mTQ2-hNTH1-YB1 Δ C-SYFP2 corresponding to Biosensor 1^{INV}). A positive FRET control corresponding to SYFP2 fused directly to mTQ2 was also prepared, which we refer to as the Fusion construct.

We first optimized the buffer conditions for measuring FRET and found that the hNTH1-YB1 Δ C interaction was salt-sensitive and was disrupted above 0.2 M NaCl (Figure 4C and Supplementary Figure 2). Indeed, the FRET efficiencies of both Biosensor 1 and Biosensor 1^{INV} were comparable to that of the Fusion positive control at 50 mM NaCl (~40%), while increasing the NaCl concentration above 200 mM led to a dramatic decrease (-30%) of the FRET efficiencies of these constructs. In contrast,

high salt concentrations only mildly affected the FRET of the Fusion construct (-5%). Biosensors 2 and 3, missing one of the two partners, respectively YB1 Δ C or hNTH1, displayed strongly reduced FRET efficiencies in low salt condition (50 mM NaCl) compared to Biosensor 1 and in the case of Biosensor 2 also increased basal FRET levels at high salt (above 200 mM) concentrations. Therefore, the change in FRET efficiency (Δ FRET) between 50 and 500 mM NaCl observed for Biosensor 1 and 1^{INV} constructs reflects a specific interaction between the two partners, hNTH1 and YB1 Δ C.

To further demonstrate that the FRET signals observed with Biosensor 1 constructs are the result of a specific interaction between hNTH1 and YB1 Δ C, we performed FRET measurements in the presence of a highly specific DNA substrate of hNTH1 (called hereafter 'THF-oligo'), a 12mer duplex containing a stable abasic site analogue tetrahydrofuran (THF) in the central position paired with guanine. Such a substrate binds to hNTH1 with nanomolar affinity.³² Addition of the DNA substrate reduced the FRET efficiencies of Biosensor 1 and 1^{INV} constructs by nearly 30%, but, as expected, had no effect on the FRET levels of the Fusion control and only a limited effect on Biosensors 2 and 3 (Figure 4D). These experiments thus confirm that the observed FRET levels of Biosensors 1 and 1^{INV} are the result of a specific interaction between hNTH1 and YB1 Δ C, and indicate that this interaction is most likely disrupted by the binding of hNTH1 to its DNA substrate. The observation that the FRET efficiency of Biosensor 3, containing solely hNTH1, did not significantly change upon addition of the DNA substrate suggests that the decrease in FRET efficiency seen with Biosensors 1 and 1^{INV} does not result from a conformational change in hNTH1 induced by substrate binding, which could have positioned the fluorescent proteins in an unfavorable configuration for FRET.

The characterization of the different Biosensor constructs thus clearly indicated that Biosensors 1 and 1^{INV} are suitable for probing the hNTH1-YB1 Δ C interaction. For subsequent experiments, we focused on the Biosensor 1 construct because the purification yield for this construct and its stability were higher compared to Biosensor 1^{INV}.

Biosensor 1 as a tool for HTS

We next evaluated the suitability of Biosensor 1 for HTS to search for chemical inhibitors of the hNTH1-YB1 Δ C complex. First, we determined the minimal amount of Biosensor 1 needed to obtain reliable FRET measurements in view of assay miniaturization in 384-well microplates (Supplementary Figure 3A). We observed that the FRET efficiency of Biosensor 1 rapidly dropped when lowering the concentration below 0.2 μ M. This was not the case with the Fusion protein, which exhibited a constant FRET efficiency irrespective of its concentration, as expected for intramolecular FRET. We thus set the Biosensor 1 concentration to 0.2 μ M in our subsequent screening experiments, corresponding to a FRET efficiency of \sim 30%.

Because compounds are typically dissolved in DMSO, we evaluated the effect of DMSO on the FRET levels of Biosensor 1 (Supplementary Figure 3B). We observed only a slight decrease in the FRET efficiency as a function of DMSO concentration indicating that high concentrations of DMSO (up to 5% DMSO) were compatible with our assay.

Next, we performed a dose response curve with the THF-oligo, which we planned to use as a bioactive control -inducing strong reduction in the FRET level of Biosensor 1- in our subsequent screening experiments. The THF-oligo was found to inhibit the hNTH1-YB1 Δ C interaction with an IC₅₀ value of 0.1 μ M (Supplementary Figure 3C). We therefore chose to use it at a final concentration of 0.5 μ M to induce maximal inhibition of the FRET signal. Finally, we examined the stability of the Biosensor 1 FRET efficiency over a 2-hour period in the presence and absence of the DNA substrate and 0.5 or 1.3% DMSO (Supplementary Figure 3D). The FRET signal of Biosensor 1 was relatively stable over time with only a slight decrease in the signal after two hours of incubation and the difference in FRET levels observed in the absence and presence of the THF-oligo remained around 20%. One of the major limitations of previously reported FRET-based biosensors is the small to medium changes in FRET signal.⁴² With the Biosensor 1, in contrast, the large change in FRET signal (~20%) makes this assay ideally suited for miniaturization and HTS.

Finally, to test the statistical robustness of our Biosensor 1-based assay, we performed a Z' factor test⁴³ on 30 technical replicates of 0.2 μ M Biosensor 1 in the absence and presence of 0.5 μ M THF-oligo. A Z' factor between 0.5 and 1.0 indicates that the assay quality is high and suitable for HTS. We obtained a Z' factor of 0.9 indicating that our Biosensor 1 is particularly well-suited for HTS. It is fast, robust, simple and low-cost.

Chemical library screening with Biosensor 1

As a pilot experiment, we screened two relatively small libraries, Life Chemicals PPI library and Prestwick Chemical library) composed of respectively 800 and 1280 compounds, that are well adapted to test the suitability of Biosensor 1 as a screening assay and are sufficiently diverse to provide us with some initial, promising hits, to define the hNTH1-YB1 interface as a druggable target in cancer therapy. Moreover, the advantage of the Prestwick Chemical library is that it contains 95% approved drugs (FDA, EMA and other agencies), which can facilitate and accelerate subsequent drug development processes. In both cases, a primary screen was performed on a robotic set-up in triplicate using a single compound concentration (50 μ M) and a confirmation of primary hits was then carried out at three compound concentrations (50, 10 and 1 μ M) each in triplicate on the 30 most potent molecules (respectively 3.75 and 2.35% of the screened compounds), which showed at least 25% inhibition. The overall results of these screens are presented in Supplementary Figure 4 and 5.

No primary hits from the Life Chemicals library were validated in the confirmation screen. Indeed, three compounds from this library (Supplementary Figure 4) were found to significantly decrease the FRET levels of Biosensor 1, but additional measurements in which the auto-fluorescence of each of these three compounds was monitored revealed that the apparent decrease in FRET efficiencies were largely due to their intrinsic fluorescence. Although our FRET measurements, like other FRET based assays,^{39-41,44,45} were performed as ratiometric assays to reduce the effects of autofluorescence and spectral interference of media and test compounds, false positives can nonetheless be selected when the autofluorescence of compounds strongly overlaps with donor emission signal. These three compounds were also found to cause a significant reduction in the FRET efficiency of the Fusion construct clearly indicating that they correspond to false positive hits (Supplementary Figure 4D).

In contrast, screening of the Prestwick Chemical library allowed us to select eight hits (corresponding to 0.60% of screened compounds) as potential inhibitors of the hNTH1-YB1ΔC complex (indicated with a star in Supplementary Figure 5). The intrinsic fluorescence of these selected compounds was verified before proceeding with further experiments. This strategy allowed us to rapidly eliminate compounds that either strongly enhanced or quenched the fluorescence signal of the fluorescent proteins used in this assay (Supplementary Figure 5). Eight compounds were selected that induced a clear dose-dependent inhibition of the FRET efficiency of Biosensor 1 with inhibition levels over 40% at 50 μM (Figure 5A). The names, properties and molecular structures of these eight compounds are provided in Supplementary Table 1. Amphotericin B is a polyene antifungal antibiotic produced by *Streptomyces nodosus*, with antifungal activity. Ceftazidime pentahydrate, cefsulodine sodium, moxalactam disodium and cefotaxime sodium are beta-lactams and cephalosporin antibiotics with bactericidal activity. Meclocycline sulfosalicylate and oxytetracycline are tetracycline derivative antibiotics. Mitoxantrone is an anthracenedione antibiotic with antineoplastic activity and a topoisomerase II inhibitor. Cefotaxime sodium was left out of the following characterization procedure because it was the least effective of the four beta-lactam antibiotics (Figure 5A).

Validation of selected hits

In order to further validate the seven selected hits, we prepared inhouse stock solutions starting from commercially available powders of amphotericin B, meclocycline sulfosalicylate, moxalactam disodium, cefsulodin sodium, mitoxantrone dihydrochloride, ceftazidime pentahydrate and oxytetracycline dihydrate. Manual FRET measurements were first performed on the Fusion construct (Supplementary Figure 5C). None of these compounds affected the FRET signal produced by the Fusion control, indicating that they do not interfere with the FRET process itself.

Next, we evaluated the inhibitory effects of the freshly prepared compounds on Biosensor 1 (Supplementary Figures 5D and 6). The inhibitory effects of these seven hits at 50 μ M were globally similar (or slightly higher) to those seen in our confirmation screen (Supplementary Figure 5D). The inhibitory effects of amphotericin B, meclocycline and oxytetracycline were the highest (>100% inhibition) surpassing the inhibitory effect of the THF-oligo. Ceftazidime, cefsulodine and mitoxantrone were found to be potent inhibitors irrespective of their source with inhibitions of ~90, ~65 and ~45% respectively. In the case of moxalactam, the fresh solution showed similar inhibitory effects as seen in our confirmation HTS screen (~60%), while the compound provided by the CMBA platform was found to be less potent in this assay, causing only a 20% inhibition. Long-term storage of this compound may have reduced its efficiency. Overall, these experiments confirmed that these seven compounds strongly inhibit Biosensor 1 FRET signal as seen in the primary and confirmation screens.

Dose-response curves (Supplementary Figure 6) were then performed with these seven confirmed hits to determine their IC_{50} values (Table 1). All seven compounds exhibited clear dose-dependent inhibition of Biosensor 1 FRET efficiency. Amphotericin B, meclocycline, ceftazidime, oxytetracycline and cefsulodine were found to be the more potent inhibitors of the hNTH1-YB1 Δ C interaction with IC_{50} values between 8 and 20 μ M (Table 1). Mitoxantrone and moxalactam exhibited higher IC_{50} values (> 30 μ M) and thus appear to be weaker inhibitors.

Finally, the inhibitory potentials of these compounds were further assessed using an orthogonal protein-protein interaction assay – the AlphaLISA assay. For six of these compounds, (amphotericin B, meclocycline, moxalactam, cefsulodin, ceftazidime and oxytetracycline), dose-dependent inhibition of the hNTH1-YB1 Δ C interaction was also detected using the AlphaLISA assay (Table 1 and Figure 5B). The dark color of Mitoxantrone precluded its use in this luminescence-based assay (due to quenching of the signal). No IC_{50} value could therefore be determined for this compound using this alternative technique. For the other compounds, IC_{50} values were obtained from the AlphaLISA assay (Table 1). These values were in a similar range to those determined using the FRET-based Biosensor 1, although slightly lower (except for amphotericin B and cefsulodine). Six compounds thus exhibited clear dose-dependent inhibition of the hNTH1-YB1 Δ C interaction using two distinct PPI assays. Of these, three compounds stand out with IC_{50} values below 20 μ M for both assays: meclocycline, ceftazidime and oxytetracycline, two of which are tetracycline derivatives, indicating that the shared tetracycline structure may be directly implicated in the inhibition process.

Molecular target of selected hits

To determine the molecular targets of each of these six compounds, we performed thermal shift assays on the individual hNTH1 and YB1 Δ C proteins in the absence and presence of a molar excess

of the selected hits. hNTH1 alone or in the presence of DMSO exhibits a melting temperature (T_m) of 55°C, which in the presence of several of these compounds was significantly increased (Figure 6A-C and Table 1). In particular, amphotericin B, cefsulodine, ceftazidime and to a lesser extent oxytetracycline clearly enhanced the thermal stability of hNTH1 – their effects were very similar to those measured upon addition of the hNTH1 DNA substrate, the THF-oligo (Figure 6A). These 4 compounds thus clearly target hNTH1. In contrast, addition of moxalactam had no detectable effect on hNTH1 and meclocycline only slightly increased the T_m of hNTH1, an effect that may be caused by its perturbation of the hNTH1 melting curve, which was much noisier than for the other measurements (Figure 6B).

YB1 Δ C, unlike hNTH1, contains several disordered domains and its melting curve was more complex, but nonetheless exhibited a distinctive shape that allowed us to derive the T_m of YB1 Δ C, which was found to be close to 37.0°C (Figure 6D-F). Upon addition of the six selected compounds, only two of these, the two tetracycline antibiotics, meclocycline and oxytetracycline, induced a noticeable change in the curve profile and the derived T_m (Figure 6D and Table 1) indicating that they interact with YB1 Δ C. Meclocycline caused the main peak of the primary derivative of the melting curve to be significantly shifted towards higher temperatures (39.5°C) and the appearance of a clear shoulder centered around 42.5°C, while oxytetracycline only caused the latter, with the appearance of a marked shoulder around 42.5°C. These observations suggest that YB1 Δ C may offer multiple binding sites for these two compounds and that these sites are not fully occupied under the experimental conditions used in the present study.

Our experiments thus indicate that amphotericin B, cefsulodine and ceftazidime clearly target hNTH1, while meclocycline binds to YB1 Δ C and oxytetracycline interacts with both proteins. Moxalactam, however, showed no detectable interaction with hNTH1 and YB1 Δ C in these assays, possibly as a result of a low affinity for its molecular target, in agreement with its lower potency as an inhibitor (highest IC_{50} values of the six selected compounds).

Sensitization of MCF7 cells to cisplatin

As mentioned in the introduction, the hNTH1-YB1 complex formation increases after exposure to cisplatin and knocking down hNTH1 or YB1 protein levels sensitizes cells to this chemotherapeutic agent.³⁰ We therefore evaluated the ability of these six compounds to restore sensitivity of MCF7 cells to cisplatin. MCF7 cells were grown for 24 or 48h in the presence of increasing amounts of cisplatin. In agreement with previous observations,³⁰ we observed that below 5 μ M cisplatin, the viability of MCF7 cells after 48h was not significantly affected. We thus chose to perform our experiments with either 5 μ M cisplatin for 48h or with 20 μ M cisplatin for 24h (Figure 7 and Supplementary Figure 7), two

concentrations that only moderately reduce the viability of MCF7 cells by 5-15% (Supplementary Figure 7). First, MCF7 cells were treated with the six selected compounds alone at various concentrations to determine their effects on MCF7 cell viability after 24 and 48h. We observed that amphotericin B and the three lactam antibiotics significantly stimulated the growth of MCF7 cells in a concentration-dependent manner at both 24 and 48h (Supplementary Figure 7). In contrast, the two tetracycline derivatives, meclocycline and oxytetracycline, had no effect on the viability of MCF7 cells (Figure 7A and Supplementary Figure 7). Next, we treated MCF7 cells with both cisplatin and the six selected compounds and measured cell viability after 48h for 5 μ M cisplatin and after 24h for 20 μ M cisplatin (Figure 7B and Supplementary Figure 7). In these conditions, the stimulatory effect of amphotericin B and the three lactam antibiotics was significantly reduced, resulting in cell viabilities close to that of control cells treated with DMSO only. Meclocycline and oxytetracycline, however, reproducibly induced a small, but significant, concentration-dependent decrease in the viability of MCF7 cells treated with 5 μ M cisplatin (Figure 7B), indicating that these compounds moderately sensitize MCF7 cells to cisplatin. A similar effect was observed with cells treated for 24h with 20 μ M cisplatin (Supplementary Figure 7). The finding that compounds disrupting the hNTH1-YB1 interaction can sensitize MCF7 cells to cisplatin strongly argues in favor that the complex, rather than the independent proteins, is responsible for cisplatin resistance of breast cancer cells. Interestingly, these two potent compounds both target YB1 Δ C, which suggests that YB1 Δ C-targeting molecules may constitute promising leads for future drug development. Taken together, these results indicate that targeting the hNTH1-YB1 complex through binding to YB1 may represent a valid strategy to fight cisplatin chemo-resistance of breast cancer cells.

CONCLUSION

Taken together, this study clearly demonstrates that the hNTH1-YB1 interface is a druggable target for the development of new therapeutic strategies to fight chemo-resistance of breast cancer cells and our results indicate that targeting the hNTH1-YB1 complex through binding to YB1 may represent a valid strategy. Moreover, our work identifies the Biosensor 1-based assay as a remarkable tool for robotic screening of chemical libraries in search for inhibitors of the hNTH1-YB1 interaction. Beyond this system, the innovative design of the Biosensor 1 construct offers a new strategy to study PPIs and to screen for potential inhibitors of other therapeutic PPI targets in a rapid, cost-effective manner.

MATERIALS AND METHODS

Cloning

The pmTQ2-N1, pSYFP2-N1 and pSYFP2-C1 plasmids were prepared by inserting the mTurquoise2 (mTQ2) and super yellow fluorescent protein (SYFP) genes kindly provided by A. Royant in place of the GFP in pEGFP-N1 and pEGFP-C1 vectors. The SYFP2-mTQ2 Fusion construct was obtained by cloning *mTQ2* into pSYFP2-C1 vector and then transferring SYFP2-mTQ2 into the bacterial expression plasmid pProexHtB. pSYFP2-C1-NLS was prepared by inserting the *SYFP2* gene in place of the *GFP* gene in the pAcGFP-Nuc (Clontech) vector that adds three copies of the NLS of the simian virus 40 large T-antigen to the C-terminus of the fluorescent protein. Human *nth1* and *yb1* cDNAs were gene synthesized (Shinegene) and full-length *nth1* and a truncated form of *yb1* (YB1 Δ C) were cloned into pmTQ2-N1 for *hnth1* and both pSYFP2-N1 and pSYFP2-C1 for *yb1* for expression in MCF7 cells. Full-length *nth1* and constructs corresponding to either the catalytic domain only (residues 90-326; hNTH1-CAT) or the N-terminal region (residues 1-89; hNTH1-NTD) were cloned into pET21a and pProexHtB respectively for bacterial expression either as single constructs or as fusion proteins with mTQ2 (hNTH1-mTQ2 and mTQ2-hNTH1). Full-length *yb1* was cloned into pProexHtB for bacterial expression and *yb1* Δ C was cloned into pProexHtB for expression as a fusion protein with SYFP2 (SYFP2-YB1 Δ C and YB1 Δ C-SYFP2). To create the Biosensor 1 (SYFP2-YB1 Δ C-hNTH1-mTQ2) construct, *SYFP2-YB1* Δ C and *hNTH1-mTQ2* constructs were amplified by PCR and cloned into pProexHtB with a 10 amino acid linker (SGGGASGGGT) between the two constructs containing a *NheI* restriction site to facilitate the cloning. A similar procedure was used for the other biosensor constructs.

Protein expression and purification

All protein constructs expressed in *E. coli* BL21 (DE3) cells possessed a TEV cleavable N-terminal hexahistidine tag. The cultures were made in LB medium with 100 $\mu\text{g mL}^{-1}$ Ampicillin and were induced with 1 mM IPTG at 20°C overnight. Cell pellets were resuspended in 50 mM Tris pH 8.0, 2 M NaCl, 2 mM MgCl₂, 0.5 mM EDTA, 0.02% (v/v) Triton, 1 mM β -mercaptoethanol (β ME) and 10% (w/v) sucrose, supplemented with EDTA-free complete protease inhibitor tablets, 1 mM PMSF, lysozyme and DNaseI (Sigma). In addition, for constructs containing YB1, S7 nuclease (Sigma) was added to the cell lysate. Cells were lysed by sonication at 4°C and the cell lysates were loaded onto 5 mL HisTrap FF columns (GE Healthcare) equilibrated in Ni Buffer A (50 mM Tris pH 8.0, 0.5 M NaCl, 2 mM MgCl₂, 0.5 mM EDTA, 0.02% Triton X-100, 10% (v/v) glycerol). His-tagged proteins were eluted with an imidazole gradient after extensive washes with Ni buffer A supplemented with 10 mM and then 50 mM imidazole. To eliminate DNA contamination, the samples were loaded onto a 5 mL HiTrap Heparin affinity column

(GE Healthcare) and eluted with a salt gradient. After removal of the His-tag by TEV protease cleavage overnight at 4°C, the samples were loaded onto a Superdex 200 10/300 GL column (GE Healthcare) equilibrated in a buffer containing 20 mM Tris pH 8.0, 500 mM NaCl, 0.2 mM EDTA, 1 mM TCEP, 10% glycerol. For the AlphaLISA assays, His-tagged hNTH1 was used – for this uncleaved protein was gel filtered. The purity of proteins was confirmed by TGX Stain-Free gel electrophoresis (Bio-Rad) at each step of the purifications and only the highly pure fractions were retained. Purified proteins were stored at -80°C.

hNTH1 activity assay

hNTH1 activity measurements were performed using 5'-FAM (fluorescein amidite) labelled 35mer duplex DNA with a thymine glycol (Tg) in position 14 described previously.³² The oligonucleotide strand containing Tg was FAM-labelled and synthesized by Midland Certified Reagent Co. and its complementary strand was purchased from MWG Eurofins. 75 nM DNA and 3 nM hNTH1 were incubated at 37°C in a master mix with 50 mM Tris pH 7.5, 150 mM NaCl, 2 mM β ME, 0.01% Triton X-100 and 0.1 mg mL⁻¹ BSA, in the presence and absence of 30 nM YB1. At each time point, 10 μ l samples were removed from the master mix and transferred to new tubes containing 10 μ l of 2X denaturing loading buffer (2X TBE, 8 M urea, 0.025% (w/v) bromophenol blue, 0.025% (w/v) SDS) and were stored on ice. At the end of the experiment, 10 μ l of each sample were transferred to a new tube with 1 μ l 1 M NaOH and heat-treated for 2 minutes in a heating block at 95°C in order to analyze the DNA glycosylase activity. The other half remained and was used to analyze AP-lyase activity. All samples were separated on 20% 8 M Urea-TBE denaturing acrylamide gels prerun for 30 min at 5 W per gel. Gels were run for 30 min at 5 W per gel in 1XTBE, and DNA bands were visualized using a ChemiDoc MP imager (Biorad) and analyzed using ImageLab (Biorad). Lanes and bands were fitted manually with the lane profile tool to quantify the bands. To determine the rates of glycosylase and AP-lyase activities, time points between 5 and 20 minutes were fitted to a linear regression in GraphPad Prism 6; the derived slopes correspond to the steady-state rates of excision.

FRET measurements *in vitro*

5 μ M hNTH1 and YB1 Δ C fused to mTQ2 and SYFP2 respectively were mixed in FRET buffer composed of 20 mM Tris pH 8.0, 50 mM NaCl, 0.2 mM EDTA, 10% glycerol in a reaction volume of 50 μ l. FRET measurements on the Fusion and Biosensor constructs were performed at a final concentration of 0.2 or 1 μ M in FRET buffer. The samples were transferred into 384-well low flange black flat bottom polystyrene microplates (Corning) and the fluorescence emission was measured with a microplate reader (CLARIOstar, BMG Labtech). Two excitation wavelengths were used: 435/15 nm to excite mTQ2, and 485/15 nm to excite SYFP2. After excitation at 435/15 nm, mTQ2 has an emission peak at 477/20

nm (I_{DD}). With FRET, another emission peak at 528/20 nm (I_{DA}) can be observed which results from the energy transferred from mTQ2 to SYFP2. When the sample is excited at 485/15 nm, an emission peak at 528/20 nm (I_{AA}) can be observed which is from the direct excitation of the acceptor, SYFP2. The FRET efficiency, E , was calculated after correction of overlapped signals by the intensity-based ratiometric method^{46,47} using the following equations:

$$E = \frac{A}{1+A} \text{ with } A = \frac{1}{\alpha} \times \frac{I_{DA} - (I_{DD} \times S_1) - (I_{AA} \times S_2) + (I_{DD} \times S_2 \times S_3)}{I_{DD}}$$

α factor was determined to be 1.37 for the mTQ2/SYFP2 FRET pair, S_1 is the contribution of the donor alone to the FRET signal (I_{DA}/I_{DD}) and was calculated to be 0.42 for mTQ2. S_2 is the contribution of the acceptor alone to the FRET signal (I_{DA}/I_{AA}) and was calculated to be 0.04 for SYFP2. S_3 is the contribution of the donor alone to the acceptor signal (I_{AA}/I_{DD}) and was calculated to be 0.04 for mTQ2.

Cell culture and transfection

MCF7 cells (ATCC HTB-22) were grown in Dulbecco's Modified Eagle's Medium (DMEM) with GlutaMAX (Gibco), supplemented with 10% FBS and 1% penicillin/streptomycin, non-essential amino acids (0.1 mM), insulin (10 $\mu\text{g mL}^{-1}$) and sodium pyruvate (1 mM). To generate the stable cell line, expressing hNTH1-mTQ2 protein, MCF7 cells were transfected with pmTQ2-N1-hNTH1 using FuGENE HD (Promega) in 35mm dishes, and subsequently diluted and selected with 1 mg mL^{-1} Geneticin G418 (Gibco). For FRET experiments, this stably transfected MCF7 cell line expressing hNTH1-mTQ2 was transiently transfected with pSYFP2-N1-YB1 Δ C, pSYFP2-C1-YB1 Δ C or pSYFP2-C1-NLS using FuGENE HD (Promega) in 35mm dishes. To assess the effects of cisplatin and selected hits on the viability of MCF7 cells, cells were seeded in 96-well clear-bottom black microplates (Greiner) with 7,000 cells per well in 80 μL of complete DMEM medium as described above. After 24-hour incubation, 10 μL of compounds or DMSO alone diluted in complete medium were added, to obtain a range of final concentrations from 50 μM to 5 μM ; then 10 μL of cisplatin diluted in sterile 0.9% (w/v) NaCl solution were added in order to obtain the desired final concentration (5 μM or 20 μM). After a 24 or 48-hour incubation, 10 μL of PrestoBlue™ cell viability reagent (Thermo Fisher) were added and fluorescence signal (Excitation at 560nm / Emission at 590 nm) was measured after a 30-minute incubation to quantify the cell viability in response to treatment. Presented data were extracted from two independent experiments each of which was performed in triplicate.

Gradual acceptor photobleaching

Gradual acceptor photobleaching experiments to detect FRET signal were performed on fixed (4% (w/v) paraformaldehyde) MCF7 cells 24 hours post-transfection. 50 sequential images were acquired using a spinning disk confocal system (Yokogawa CSUX1 head, Olympus IX81 microscope, and Andor

iXon Ultra EMCCD camera) at 100 ms exposure time, using AOTF controlled lasers at 445 nm (40 mW) for mTQ2 with 80% power and at 515 nm (50 mW) for SYFP2 with 5% power. After 10 acquired images, the acceptor was gradually photobleached (100 ms exposure time, laser 515 nm and 1-3% power) in a selected area of the nucleus using a FRAPPA device (Fluorescence recovery after photobleaching (FRAP) and photoactivation (PA); Andor). Images were analyzed to calculate FRET efficiencies using the acceptor photobleaching (donor dequenching) method described previously,⁴⁸ which is independent of the donor-to-acceptor ratio. Briefly, we used Volocity™ (Quorum Technologies) to measure the background corrected mean intensities of the donor (I_D) and the acceptor (I_A) channels in the photobleached region – ROI1, and a control non-bleached region – ROI2, expressed after normalization to the intensity of each channel before photobleaching. We then calculated I'_D and I'_A as the corrected values of I_D and I_A in ROI1 to account for the fluorescence intensity decay linked to imaging, using the intensities of both channels in the control area (ROI2). FRET efficiency E is then calculated as $E = I'_D - 1$, where I'_D is the coefficient of the linear regression ($I'_D = \alpha I'_A + I'_0$, σ^2) of the normalized intensity variations of the donor in ROI1 as a function of the acceptor intensities. The slope, α , is the apparent intensity ratio between the donor and the acceptor in the target cell. The correlation coefficient σ^2 was used to estimate the validity of each calculated FRET efficiency value.

Robotic high-throughput screening

Screen reliability and robustness was evaluated by estimating the Z' factor.⁴³ For this, the FRET efficiencies of 30 technical replicates of the Biosensor 1 (0.2 μ M) alone as positive control and in the presence of 0.5 μ M THF-oligo as negative 'bioactive' control (12mer dsDNA oligonucleotide with a tetrahydrofuran in position 7 paired with a guanine: 5'-TGTCCAXGTCTC-3' with X=THF and complementary strand: 5'-GAGACGTGGACA-3') in FRET buffer were measured. Z' factor was calculated using the following formula:

$$Z' = 1 - \frac{(3 \text{ SD of positive controls} + 3 \text{ SD of negative controls})}{|\text{mean of positive controls} - \text{mean of negative controls}|}$$

For HTS, Biosensor 1 protein at a final concentration of 0.2 μ M in FRET buffer was transferred into 384-well low-flange black flat-bottom polystyrene microplate (Corning) using the robotic set-up of the CMBA platform. Each compound from the Life Chemicals PPI library and the Prestwick Chemical library was then added at a final concentration of 50 μ M in the FRET buffer supplemented with either 1.3 or 0.5% (v/v) DMSO, respectively. Each molecule was tested in triplicate. Positive control wells (9/384 per assay plate) contained Biosensor 1 in 1.3% (v/v) DMSO for Life Chemicals and 0.5% DMSO for Prestwick Library and negative control wells (3/384 per assay plate) contained Biosensor 1 with 0.5 μ M THF-oligo. Fluorescence in each well was measured with a TECAN Infinite® M1000 microplate reader at different timepoints after preparing the reactions: 15, 30 and 60 minutes. Only the 60-minute

measurements are presented in this study. Confirmation screens were performed with 30 selected compounds from the primary screening at three different compound concentrations (50, 10 and 1 μM) in triplicate.

Validation experiments

Selected hits from our secondary HTS were ordered from Sigma and 10 mM stock solutions were prepared in 100% DMSO. When stock solutions were used immediately after preparation (or after thawing aliquots stored at -20°C), their inhibitory effects were significantly reduced. Storage of the compounds at 4°C for at least 7 days was necessary to reproduce the results of the HTS experiments. UV/Vis absorbance spectra of the compounds were performed on a Nanodrop spectrophotometer immediately after preparation and after storage at 4°C , and were compared to that of compounds provided by the CMBA screening platform and used for the HTS (Supplementary Fig. S8). For several compounds, substantial changes in these spectra were observed upon storage of the compound at 4°C . This may be caused by low solubility or poor stability of these compounds. The active compounds in these stored solutions may indeed correspond to modified forms of the expected chemicals, which would explain their enhanced inhibitory potential after storage. Such compound loss or instability during storage has previously been reported.⁴⁹ For the validation experiments (dose-response experiments using Biosensor 1 or AlphaLISA assay), only the active compounds stored at 4°C were used. Compounds were serially diluted in reaction buffer supplemented with 1% DMSO. Dose-response curves were established by measuring the FRET (as described above) on 50 μl reactions containing 0.2 μM Biosensor 1 in FRET buffer in the presence of 0-100 μM compound or DMSO alone. The data points corresponding to the means of triplicate measurements were fitted to a four-parameter sigmoidal inhibition model in GraphPad Prism 8: ($Y = Bottom + (Top - Bottom) / [1 + (\frac{IC_{50}}{X})^{HillSlope}]$). Reliable IC_{50} values could be determined for all compounds except moxalactam for which only partial inhibition of the FRET signal was achieved at the highest concentration.

AlphaLISA measurements

Donor beads coated with streptavidin and AlphaLISA acceptor beads coated with anti-His antibodies were used to bind biotinylated YB1 ΔC and His-tagged hNTH1, respectively. To biotinylate YB1 ΔC , 0.5 mg YB1 ΔC was transferred into a phosphate buffer (20 mM NaPhosphate pH 8.0, 0.5 M NaCl, 1 mM MgCl_2 , 5% glycerol, 0.005% Triton X-100 and 1 mM βME) using a 5 mL HiTrap Desalting column (GE Healthcare). YB1 ΔC was then incubated with 0.25 mM NHS-Biotin (Sigma) at 25°C for 2 hours before the reaction was stopped by the addition of 50 mM Tris pH 8.0. The excess of NHS-Biotin was then removed by a second run on the desalting column equilibrated in 20 mM Tris pH 8.0, 500 mM NaCl,

0.2 mM EDTA, 1 mM TCEP, 10% glycerol. Fractions containing biotinylated YB1ΔC were pooled, aliquoted and stored at -80°C. AlphaLISA assays were performed in white, flat-bottom, small volume 384-well plates (Perkin Elmer). The final reaction volume was 20 μL including 8 μL AlphaLISA buffer (composed of 20 mM Tris pH 7.5, 150 mM NaCl, 0.01% Triton X-100, 0.01% (v/v) Tween 20, 0.5 mM EDTA, 1 mM βME and 0.1 mg mL⁻¹ BSA), 2 μL biotinylated YB1ΔC (100 nM), 2 μL His-tagged hNTH1 (1 μM), 4 μL acceptor beads (0.1 mg mL⁻¹) and 4 μL donor beads (0.1 mg mL⁻¹). All reagents were diluted in AlphaLISA buffer. The plate was read on the CLARIOstar plate-reader (BMG Labtech) fitted with an aperture spoon (to avoid excitation of neighboring wells) and the appropriate filters (excitation filter at 680/40 nm and emission filter at 570/100 nm). Reactions were prepared in triplicate. To estimate the apparent binding affinity of the hNTH1-YB1ΔC complex, increasing amounts of untagged hNTH1 diluted in AlphaLISA buffer was titrated into the AlphaLISA reactions in place of the 8 μL of buffer. For dose-response experiments, with selected hits, the latter were diluted in AlphaLISA buffer supplemented with 1% DMSO and were also titrated into the reactions in place of the 8 μL of buffer. The data points corresponding to the means of triplicate measurements were fitted to a three-parameter sigmoidal inhibition model ($Y = Bottom + (Top - Bottom) / [1 + (\frac{X}{IC50})]$) in GraphPad Prism 8, except for the amphotericin B data for which a four-parameter sigmoidal inhibition model was used ($Y = Bottom + (Top - Bottom) / [1 + (\frac{IC50}{X})^{HillSlope}]$), with a Hill Slope value of -1.81.

Thermal shift assay

Thermal shift assays were carried out as described previously.⁵⁰ hNTH1 at a final concentration of 5 μM and YB1ΔC at a final concentration of 15 μM were incubated with respectively 100 μM or 150 μM compounds (or DMSO alone) in 20 mM Tris pH 8.0, 50 mM NaCl and 5 % glycerol for 1 hour at room temperature before addition of Sypro Orange 8X. 25 μL reactions were then distributed in 0.2 mL PCR-strips that were placed in a real-time qPCR machine (Bio-rad) and heated from 20 to 90°C with temperature increments of 0.5°C/min. The fluorescence signal of the Sypro Orange was recorded at each step and the T_m values were determined using the primary derivatives of the fluorescence signal. Presented data were extracted from two independent experiments each of which was performed in triplicate.

Statistical analysis

Statistical tests were performed with GraphPad Prism 6 and 8. *P* values below 0.05 were considered as significant and are indicated in figures with asterisks as follows: * 0.01 < *P* < 0.05; ** 0.001 < *P* < 0.01; *** 0.0001 < *P* < 0.001; **** *P* < 0.0001.

ASSOCIATED CONTENT

The Supporting Information is available free of charge online. This includes Supplemental Table S1 and supplemental Figures S1 to S8.

FUNDING

This work has been supported by the LabEx GRAL (ANR-10-LABX-49-01), the Fondation ARC (PJA 20151203255), the Fondation de France (N° 2012-00034094) and the Radiobiology segment of the CEA. MS was supported by the Scientific and Technological Research Council of Turkey (TUBITAK 2214/B International Joint PhD Fellowship Programme). This work used the platforms of the Grenoble Instruct-ERIC Center (ISBG: UMS 3518 CNRS-CEA-UGA-EMBL) with support from FRISBI (ANR-10-INBS-05-02) and GRAL (ANR-10-LABX-49-01) within the Grenoble Partnership for Structural Biology (PSB). Part of this work was also performed at the GAP2D-CMBA screening platform, which is a member of the GIS-IBISA and the ChemBioFrance infrastructure.

ACKNOWLEDGEMENTS

We thank B. Tosun and F. Chancel for technical assistance for the *in vitro* and *in cellulo* validation of the selected hits and A.-M. Villard for help with the thermal shift assay. We thank T. W. J. Gadella (Swammerdam Institute for Life Sciences, University of Amsterdam) and A. Royant (Institut de Biologie Structurale, Grenoble) for providing us with mTurquoise2 and SYFP2 genes.

REFERENCES

- (1) Sancar, A., Lindsey-Boltz, L. A., Ünsal-Kaçmaz, K., and Linn, S. (2004) Molecular Mechanisms of Mammalian DNA Repair and the DNA Damage Checkpoints. *Annu. Rev. Biochem.* **73**, 39–85.
- (2) Hoeijmakers, J. H. (2001) Genome maintenance mechanisms for preventing cancer. *Nature* **411**, 366–374.
- (3) Tubbs, A., and Nussenzweig, A. (2017) Endogenous DNA Damage as a Source of Genomic Instability in Cancer. *Cell* **168**, 644–656.
- (4) Krokan, H. E., and Bjoras, M. (2013) Base excision repair. *Cold Spring Harb Perspect Biol* **5**, a012583.
- (5) Dizdaroglu, M. (2015) Oxidatively induced DNA damage and its repair in cancer. *Mutat. Res. Mutat. Res.* **763**, 212–245.
- (6) Madhusudan, S., Smart, F., Shrimpton, P., Parsons, J. L., Gardiner, L., Houlbrook, S., Talbot, D. C., Hammonds, T., Freemont, P. A., Sternberg, M. J. E., Dianov, G. L., and Hickson, I. D. (2005) Isolation of a small molecule inhibitor of DNA base excision repair. *Nucleic Acids Res.* **33**, 4711–4724.
- (7) Dianov, G. L. (2011) Base excision repair targets for cancer therapy. *Am. J. Cancer Res.* **1**, 845–851.
- (8) Malyuchenko, N. V., Kotova, E. Y., Kulaeva, O. I., Kirpichnikov, M. P., and Studitskiy, V. M. (2015) PARP1 Inhibitors: antitumor drug design. *Acta Naturae* **7**, 27–37.
- (9) Dizdaroglu, M. (2005) Base-excision repair of oxidative DNA damage by DNA glycosylases. *Mutat Res* **591**, 45–59.
- (10) Liu, X., Choudhury, S., and Roy, R. (2003) In Vitro and in Vivo Dimerization of Human Endonuclease III Stimulates Its Activity. *J. Biol. Chem.* **278**, 50061–50069.

- (11) Liu, X., and Roy, R. (2002) Truncation of amino-terminal tail stimulates activity of human endonuclease III (hNTH1). *J. Mol. Biol.* 321, 265–276.
- (12) Bessho, T. (1999) Nucleotide excision repair 3' endonuclease XPG stimulates the activity of base excision repair enzyme thymine glycol DNA glycosylase. *Nucleic Acids Res.* 27, 979–983.
- (13) Klungland, A., Höss, M., Gunz, D., Constantinou, A., Clarkson, S. G., Doetsch, P. W., Bolton, P. H., Wood, R. D., and Lindahl, T. (1999) Base Excision Repair of Oxidative DNA Damage Activated by XPG Protein. *Mol. Cell* 3, 33–42.
- (14) Marenstein, D. R., Chan, M. K., Altamirano, A., Basu, A. K., Boorstein, R. J., Cunningham, R. P., and Teebor, G. W. (2003) Substrate Specificity of Human Endonuclease III (hNTH1): Effect of Human APE1 on hNTH1 Activity. *J. Biol. Chem.* 278, 9005–9012.
- (15) Marenstein, D. R., Ocampo, M. T., Chan, M. K., Altamirano, A., Basu, A. K., Boorstein, R. J., Cunningham, R. P., and Teebor, G. W. (2001) Stimulation of human endonuclease III by Y box-binding protein 1 (DNA-binding protein B). Interaction between a base excision repair enzyme and a transcription factor. *J Biol Chem* 276, 21242–21249.
- (16) Kohno, K., Izumi, H., Uchiumi, T., Ashizuka, M., and Kuwano, M. (2003) The pleiotropic functions of the Y-box-binding protein, YB-1. *BioEssays* 25, 691–698.
- (17) Lasham, A., Print, C. G., Woolley, A. G., Dunn, S. E., and Braithwaite, A. W. (2013) YB-1: oncoprotein, prognostic marker and therapeutic target? *Biochem J* 449, 11–23.
- (18) Kim, A., Shim, S., Kim, Y., Kim, M.-J., Park, S., and Myung, J. K. (2020) Inhibition of Y box binding protein 1 suppresses cell growth and motility in colorectal cancer. *Mol. Cancer Ther.* 19, 479-489.
- (19) Zheng, H., Zhan, Y., Zhang, Y., Liu, S., Lu, J., yang, Y., Wen, Q., and Fan, S. (2019) Elevated expression of G3BP1 associates with YB1 and p-AKT and predicts poor prognosis in nonsmall cell lung cancer patients after surgical resection. *Cancer Med.* 8, 6894–6903.
- (20) Ohga, T., Koike, K., Ono, M., Makino, Y., Itagaki, Y., Tanimoto, M., Kuwano, M., and Kohno, K. (1996) Role of the human Y box-binding protein YB-1 in cellular sensitivity to the DNA-damaging agents cisplatin, mitomycin C, and ultraviolet light. *Cancer Res* 56, 4224–4228.
- (21) Bargou, R. C., Jurchott, K., Wagener, C., Bergmann, S., Metzner, S., Bommert, K., Mapara, M. Y., Winzer, K. J., Dietel, M., Dorken, B., and Royer, H. D. (1997) Nuclear localization and increased levels of transcription factor YB-1 in primary human breast cancers are associated with intrinsic MDR1 gene expression. *Nat Med* 3, 447–450.
- (22) Janz, M., Harbeck, N., Dettmar, P., Berger, U., Schmidt, A., Jurchott, K., Schmitt, M., and Royer, H. D. (2002) Y-box factor YB-1 predicts drug resistance and patient outcome in breast cancer independent of clinically relevant tumor biologic factors HER2, uPA and PAI-1. *Int J Cancer* 97, 278–282.
- (23) Oda, Y., Ohishi, Y., Saito, T., Hinoshita, E., Uchiumi, T., Kinukawa, N., Iwamoto, Y., Kohno, K., Kuwano, M., and Tsuneyoshi, M. (2003) Nuclear expression of Y-box-binding protein-1 correlates with P-glycoprotein and topoisomerase II alpha expression, and with poor prognosis in synovial sarcoma. *J. Pathol.* 199, 251–258.
- (24) Rubinstein, D. B., Stortchevoi, A., Boosalis, M., Ashfaq, R., and Guillaume, T. (2002) Overexpression of DNA-binding Protein B Gene Product in Breast Cancer as Detected by in Vitro-generated Combinatorial Human Immunoglobulin Libraries. *Cancer Res.* 62, 4985-4991.
- (25) Yahata, H., Kobayashi, H., Kamura, T., Amada, S., Hirakawa, T., Kohno, K., Kuwano, M., and Nakano, H. (2002) Increased nuclear localization of transcription factor YB-1 in acquired cisplatin-resistant ovarian cancer. *J Cancer Res Clin Oncol* 128, 621–626.
- (26) Dahl, E., En-Nia, A., Wiesmann, F., Krings, R., Djudjaj, S., Breuer, E., Fuchs, T., Wild, P. J., Hartmann, A., Dunn, S. E., and Mertens, P. R. (2009) Nuclear detection of Y-boxprotein-1 (YB-1) closely associates with progesterone receptor negativity and is a strong adverse survival factor in human breast cancer. *BMC Cancer* 9, 410.
- (27) Eliseeva, I. A., Kim, E. R., Guryanov, S. G., Ovchinnikov, L. P., and Lyabin, D. N. (2011) Y-box-binding protein 1 (YB-1) and its functions. *Biochem.-Mosc.* 76, 1402–1433.
- (28) Sorokin, A. V., Selyutina, A. A., Skabkin, M. A., Guryanov, S. G., Nazimov, I. V., Richard, C., Th'ng, J., Yau, J., Sorensen, P. H., Ovchinnikov, L. P., and Evdokimova, V. (2005) Proteasome-mediated

cleavage of the Y-box-binding protein 1 is linked to DNA-damage stress response. *EMBO J* 24, 3602–3612.

(29) Wu, Y., Wang, K. Y., Li, Z., Liu, Y. P., Izumi, H., Uramoto, H., Nakayama, Y., Ito, K., and Kohno, K. (2014) Y-box binding protein 1 enhances DNA topoisomerase 1 activity and sensitivity to camptothecin via direct interaction. *J Exp Clin Cancer Res* 33, 112.

(30) Guay, D., Garand, C., Reddy, S., Schmutte, C., and Lebel, M. (2008) The human endonuclease III enzyme is a relevant target to potentiate cisplatin cytotoxicity in Y-box-binding protein-1 overexpressing tumor cells. *Cancer Sci* 99, 762–769.

(31) Ocampo-Hafalla, M. T., Altamirano, A., Basu, A. K., Chan, M. K., Ocampo, J. E. A., Cummings, A., Boorstein, R. J., Cunningham, R. P., and Teebor, G. W. (2006) Repair of thymine glycol by hNth1 and hNeil1 is modulated by base pairing and cis–trans epimerization. *DNA Repair* 5, 444–454.

(32) Sarre, A., Stelter, M., Rollo, F., De Bonis, S., Seck, A., Hognon, C., Ravanat, J.-L., Monari, A., Dehez, F., Moe, E., and Timmins, J. (2019) The three Endonuclease III variants of *Deinococcus radiodurans* possess distinct and complementary DNA repair activities. *DNA Repair* 78, 45–59.

(33) Kremers, G.-J., Goedhart, J., van Munster, E. B., and Gadella, T. W. J. (2006) Cyan and Yellow Super Fluorescent Proteins with Improved Brightness, Protein Folding, and FRET Förster Radius. *Biochemistry* 45, 6570–6580.

(34) Goedhart, J., von Stetten, D., Noirclerc-Savoye, M., Lelimosin, M., Joosen, L., Hink, M. A., van Weeren, L., Gadella, T. W., and Royant, A. (2012) Structure-guided evolution of cyan fluorescent proteins towards a quantum yield of 93%. *Nat Commun* 3, 751.

(35) Wells, J. A., and McClendon, C. L. (2007) Reaching for high-hanging fruit in drug discovery at protein–protein interfaces. *Nature* 450, 1001–1009.

(36) Basse, M. J., Betzi, S., Bourgeas, R., Bouzidi, S., Chetrit, B., Hamon, V., Morelli, X., and Roche, P. (2013) 2P21db: a structural database dedicated to orthosteric modulation of protein–protein interactions. *Nucleic Acids Res* 41, D824–827.

(37) Milhas, S., Raux, B., Betzi, S., Derviaux, C., Roche, P., Restouin, A., Basse, M.-J., Rebuffet, E., Lugari, A., Badol, M., Kashyap, R., Lissitzky, J.-C., Eydoux, C., Hamon, V., Gourdel, M.-E., Combes, S., Zimmermann, P., Aurrand-Lions, M., Roux, T., Rogers, C., Müller, S., Knapp, S., Trinquet, E., Collette, Y., Guillemot, J.-C., and Morelli, X. (2016) Protein–Protein Interaction Inhibition (2P21)-Oriented Chemical Library Accelerates Hit Discovery. *ACS Chem. Biol.* 11, 2140–2148.

(38) Glickman, J. F., Wu, X., Mercuri, R., Illy, C., Bowen, B. R., He, Y., and Sills, M. (2002) A comparison of ALPHAScreen, TR-FRET, and TRF as assay methods for FXR nuclear receptors. *J. Biomol. Screen.* 7, 3–10.

(39) Song, Y., Madahar, V., and Liao, J. (2011) Development of FRET Assay into Quantitative and High-throughput Screening Technology Platforms for Protein–Protein Interactions. *Ann. Biomed. Eng.* 39, 1224–1234.

(40) Schaap, M., Hancock, R., Wilderspin, A., and Wells, G. (2013) Development of a steady-state FRET-based assay to identify inhibitors of the Keap1-Nrf2 protein–protein interaction. *Protein Sci.* 22, 1812–1819.

(41) Wei, Z.-H., Chen, H., Zhang, C., and Ye, B.-C. (2014) FRET-Based System for Probing Protein–Protein Interactions between σR and RsrA from *Streptomyces Coelicolor* in Response to the Redox Environment. *PLOS ONE* 9, e92330.

(42) Tamura, T., and Hamachi, I. (2014) Recent Progress in Design of Protein-Based Fluorescent Biosensors and Their Cellular Applications. *ACS Chem. Biol.* 9, 2708–2717.

(43) Zhang, J., Chung, T., and Oldenburg, K. (1999) A Simple Statistical Parameter for Use in Evaluation and Validation of High Throughput Screening Assays. *J. Biomol. Screen.* 4, 67–73.

(44) Rogers, M. S., Cryan, L. M., Habeshian, K. A., Bazinet, L., Caldwell, T. P., Ackroyd, P. C., and Christensen, K. A. (2012) A FRET-Based High Throughput Screening Assay to Identify Inhibitors of Anthrax Protective Antigen Binding to Capillary Morphogenesis Gene 2 Protein. *PLOS ONE* 7, e39911.

(45) Chakraborty, S., Núñez, D., Hu, S.-Y., Domingo, M. P., Pardo, J., Karmenyan, A., Eva Ma Gálvez, and Chiou, A. (2014) FRET Based Quantification and Screening Technology Platform for the Interactions of

Leukocyte Function-Associated Antigen-1 (LFA-1) with InterCellular Adhesion Molecule-1 (ICAM-1). *PLOS ONE* 9, e102572.

(46) Nagy, P., Vámosi, G., Bodnár, A., Lockett, S. J., and Szöllősi, J. (1998) Intensity-based energy transfer measurements in digital imaging microscopy. *Eur. Biophys. J.* 27, 377–389.

(47) Roszik, J., Lisboa, D., Szöllősi, J., and Vereb, G. (2009) Evaluation of intensity-based ratiometric FRET in image cytometry—Approaches and a software solution. *Cytometry A* 75A, 761–767.

(48) Roszik, J., Tóth, G., Szöllősi, J., and Vereb, G. (2013) Validating Pharmacological Disruption of Protein–Protein Interactions by Acceptor Photobleaching FRET Imaging, in *Target Identification and Validation in Drug Discovery: Methods and Protocols* (Moll, J., and Colombo, R., Eds.), pp 165–178. Humana Press, Totowa, NJ.

(49) Cheng, X., Hochlowski, J., Tang, H., Hepp, D., Beckner, C., Kantor, S., and Schmitt, R. (2003) Studies on Repository Compound Stability in DMSO under Various Conditions. *J. Biomol. Screen.* 8, 292–304.

(50) Andreotti, G., Monticelli, M., and Cubellis, M. V. (2015) Looking for protein stabilizing drugs with thermal shift assay. *Drug Test. Anal.* 7, 831–834.

Table 1. Characterization of the inhibitory potential and molecular targets of selected Prestwick hits.

Compound	IC ₅₀ (μM) Biosensor 1 assay	IC ₅₀ (μM) AlphaLISA assay	T _m hNTH1 (°C)	T _m YB1ΔC (°C)
DMSO	ND	ND	55.00 ± 0.00	37.20 ± 0.76
Amphotericin B	9.55 ± 0.47	25.00 ± 4.01	58.83 ± 0.29	37.42 ± 0.74
Cefsulodine	8.94 ± 0.39	42.92 ± 11.76	59.50 ± 0.00	36.70 ± 0.45
Ceftazidime	15.36 ± 4.70	4.65 ± 0.80	59.17 ± 0.29	36.70 ± 1.04
Moxalactam	75.29 ± 177.30	19.36 ± 3.61	55.50 ± 0.00	37.00 ± 0.71
Meclocycline	19.48 ± 2.64	1.54 ± 0.26	56.17 ± 1.04	39.50 ± 1.08/42.75 ± 1.32
Oxytetracycline	17.94 ± 5.07	10.35 ± 2.89	57.67 ± 0.29	37.50 ± 0.41/42.63 ± 0.75
Mitoxantrone	31.88 ± 1.62	ND	ND	ND

ND: not determined.

Figure legends

Figure 1. Schematic illustration of the bifunctional reaction mechanism catalyzed by hNTH1 and the effect of XPG, APE1, and YB1 on the regulation of its activity. During the first glycosylase reaction, the enzyme (E) associates with its substrate DNA (DNA_{ox}) to generate an enzyme-substrate complex (E*DNA_{ox}), which leads to the removal of the oxidized base and the formation of an enzyme-abasic site complex (E*DNA_{AP}). In turn, this complex is further processed by the lyase reaction to an enzyme-nicked DNA complex (E*DNA_n) and finally, the fully processed DNA product after β-elimination is released from the enzyme (E+DNA_n). In case the two reaction steps are uncoupled, the enzyme

dissociates from the abasic site DNA ($E+DNA_{AP}$) after the glycosylase reaction, thereby creating a mixture of DNA substrates containing either abasic sites or oxidized bases. The enzyme can then engage in either one of the two sub-pathways: (i) a new round of DNA glycosylase activity on DNA_{ox} or (ii) AP-lyase activity on DNA_{AP} . The relative engagement into one or the other pathway is regulated by the abundance of the various species (E , DNA_{ox} , DNA_{AP} and DNA_n) in the reaction and by various factors. \rightarrow and \leftarrow denote stimulation and inhibition, respectively.

Figure 2. hNTH1-YB1 interaction. (A) Left: Time course experiments of the DNA glycosylase (dotted line) and lyase activities (full line) of 3 nM hNTH1 on 75 nM 35 mer dsDNA containing thymine glycol (Tg) in position 14 and a fluorescein labeled DNA substrate in the absence (black) and presence (red) of 30 nM YB1. The graphs represent the mean of three replicates and error bars are the standard deviation. Right: Table presenting the glycosylase and bifunctional (glycosylase/AP-lyase) rates (nM/min) derived from the linear region of the curves (5 to 20 min) using GraphPad Prism 6. (B) Left: AlphaLISA titration of increasing amounts (0, 25, 100, 250 and 1000 nM) of hNTH1 (WT, wild-type; hNTH1-CAT, residues 90-326; hNTH1-NTD, residues 1-89) into reactions containing 10 nM biotinylated YB1 Δ C. Right: AlphaLISA titration of increasing amounts (0, 1, 5, 10 and 50 nM) of wild-type (WT) and nuclear YB1 (YB1 Δ C, residues 1-219) into reactions containing 100 nM His-tagged hNTH1. The histograms represent the mean of three replicates and error bars are the standard deviation. The binding profiles are typical of specific binding. The reduced signal obtained at the highest concentration of proteins is due to a saturation of the binding sites on the streptavidin coated donor beads. (C) AlphaLISA competition assay. Increasing concentrations of hNTH1 (without His-tag) were added to a reaction containing 10 nM biotinylated YB1 Δ C and 100 nM His-hNTH1. The data points correspond to the mean of three replicates and error bars are the standard deviation. The untagged hNTH1 replaces the His-tagged hNTH1 in the complex leading to a decrease in the AlphaLISA signal. The data were fitted to a standard sigmoidal inhibition model in GraphPad Prism 6 and the derived IC_{50} was found to be 0.4 μ M providing an estimate of the apparent binding affinity of the YB1 Δ C-hNTH1 complex.

Figure 3. *In vitro* and *in cellulo* FRET analysis of the hNTH1-YB1 Δ C interaction. (A) *In vitro* FRET efficiencies of protein mixtures containing mTQ2 alone, mTQ2-hNTH1 or hNTH1-mTQ2 mixed with SYFP2-YB1 Δ C or YB1 Δ C-SYFP2 at 5 μ M final concentration in FRET buffer. The highest FRET signal was obtained with the fluorescent proteins fused to the C-termini of hNTH1 and YB1 Δ C. The histograms represent the mean of three replicates and error bars correspond to the standard deviation. (B)-(D) hNTH1/YB1 Δ C FRET measurements *in cellulo*. Stably transfected MCF7 cells expressing hNTH1-mTQ2 were transfected with either SYFP2-NLS alone (B), SYFP2-YB1 Δ C (C) or YB1 Δ C-SYFP2 (D). mTQ2 is seen in the CFP channel (blue). SYFP2 is seen in the YFP channel (green). *In cellulo* FRET measurements were

performed using the acceptor photobleaching method. The white rectangle indicates the area of the nucleus that was photobleached by the FRAPPA device in the images. Scale bar: 10 μm . Right panel: Normalized fluorescence intensities of the acceptor (SYFP2) and donor (mTQ2) fluorophores recorded during the FRET experiment. Photobleaching of the acceptor was initiated after the acquisition of 10 images. The calculated FRET efficiency (E_{FRET}) for each of these experiments is provided. (E) Mean FRET efficiencies in the MCF7 stable cell line expressing hNTH1-mTQ2 and transfected with either SYFP2-NLS (N=3), SYFP2-YB1 Δ C (N=3) or YB1 Δ C-SYFP2 (N=8). The presented data are the mean of at least three replicates and error bars indicate standard deviation. Data in the graphs A and E were analyzed by unpaired *t* test with GraphPad Prism 6 (* 0.01<*P*<0.05; ** 0.001<*P*<0.01; *** 0.0001<*P*<0.001; **** *P*<0.0001).

Figure 4. Design and optimization of a FRET-based biosensor. (A) Illustration of the Biosensor design. The yellow and blue cylinders represent SYFP2 and mTQ2 proteins, respectively. Upon interaction of hNTH1 with YB1 Δ C, mTQ2 and SYFP2 come close together and energy transfer between the FRET donor and FRET acceptor occurs and can be measured. (B) Illustration of the different Biosensor and Fusion constructs used in this study. Orange: N-terminal, cleavable His-tag. Grey: short linker sequences. (C) Comparison of the FRET efficiencies of 1 μM Biosensor and Fusion constructs in FRET buffers containing either 50 mM (blue) or 500 mM (red) NaCl concentrations. (D) Comparison of the FRET efficiencies of 1 μM Biosensor and Fusion constructs in absence (blue) and presence (green) of 1 μM THF-oligo in FRET buffer containing 50 mM NaCl. (C)-(D) Plotted histograms are the mean of three replicates and error bars represent the standard deviation.

Figure 5. Identification and characterization of selected hits. (A) Extent of Biosensor 1 FRET inhibition by 8 selected compounds (blue: amphotericin B, red: meclocycline, green: moxalactam, purple: cefsulodine, grey: mitoxantrone, orange: ceftazidime, brown: oxytetracycline, dark blue: cefotaxime) at 50, 10 and 1 μM compound concentrations respectively. Plotted histograms are the mean of three replicates and error bars represent the standard deviation. (B) Dose-dependent inhibition of the hNTH1- YB1 Δ C interaction by amphotericin B (blue), meclocycline (red), moxalactam (green), cefsulodine (purple), ceftazidime (orange) and oxytetracycline (brown), probed using the AlphaLISA assay. The data points corresponding to the means of triplicate measurements were fitted to a three-parameter sigmoidal inhibition model in GraphPad Prism 8, except for the amphotericin B data for which a four-parameter sigmoidal inhibition model was used with a *Hill Slope* value of -1.81.

Figure 6. Characterization of the molecular targets of selected hits. (A)-(C) Effects of the selected compounds (100 μM), DMSO only (1%) or the THF-oligo (20 μM) on the melting temperature of 5 μM

hNTH1. (A)-(B) Normalized primary derivatives of the melting curves of hNTH1 in the presence of compounds that either significantly shift the T_m values of hNTH1 (A) or for which no obvious change in the T_m was observed (B). The mean T_m values of hNTH1 derived from these graphs are shown in (C). The data points correspond to the mean of at least 3 replicates and the error bars correspond to the standard deviation. (D)-(F) Effects of the selected compounds (150 μM), DMSO only (1.5%) or the THF-oligo (30 μM) on the melting temperature of 15 μM YB1 Δ C. (D)-(E) Normalized primary derivatives of the melting curves of YB1 Δ C in the presence of compounds that either significantly shift the T_m values of YB1 Δ C (D) or for which no obvious change in the T_m was observed (E). The mean T_m values of YB1 Δ C derived from these graphs are shown in (F). The data points correspond to the mean of at least 3 replicates and the error bars correspond to the standard deviation. In the presence of meclocycline and oxytetracycline, the primary derivative of the melting curve of YB1 Δ C exhibited two peaks (arrows in panel D), hence the two histograms for these compounds in (F). The histogram corresponding to the second peak/shoulder is illustrated with a checkered pattern. (C) and (F): Statistical analysis was performed using a one-way ANOVA test (Dunnett's test) in GraphPad Prism 8 (ns: non-significant, * $0.01 < P < 0.05$; ** $0.001 < P < 0.01$; *** $0.0001 < P < 0.001$; **** $P < 0.0001$).

Figure 7. Effects of selected hits on the sensitivity of MCF7 cells to cisplatin. (A) Relative viability of MCF7 cells treated with either 5 to 50 μM DMSO (black), meclocycline (red) or oxytetracycline (brown) for 24h. (B) Relative viability of MCF7 cells treated with 5 μM cisplatin supplemented with either 5 to 50 μM DMSO (black), meclocycline (red) or oxytetracycline (brown) for 24h. Plotted histograms are the mean of four replicates and error bars represent the standard deviation. The viability of DMSO treated cells at each concentration was set to 100% and was used as a reference for calculating the relative viability of compound-treated cells. Statistical analysis performed using a one-way ANOVA test (Dunnett's test) in GraphPad Prism 8 revealed that the concentration-dependent decrease in cell viability induced by meclocycline and oxytetracycline in the presence of cisplatin was significant (ns: non-significant, * $0.01 < P < 0.05$; ** $0.001 < P < 0.01$).

Figure 1

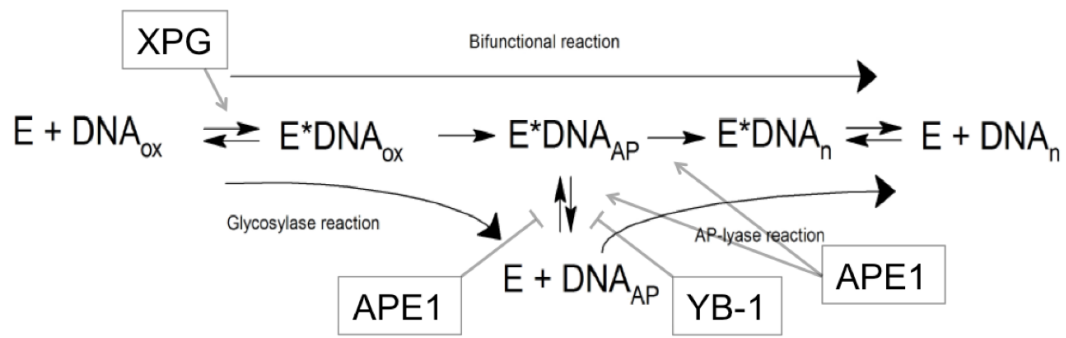


Figure 2

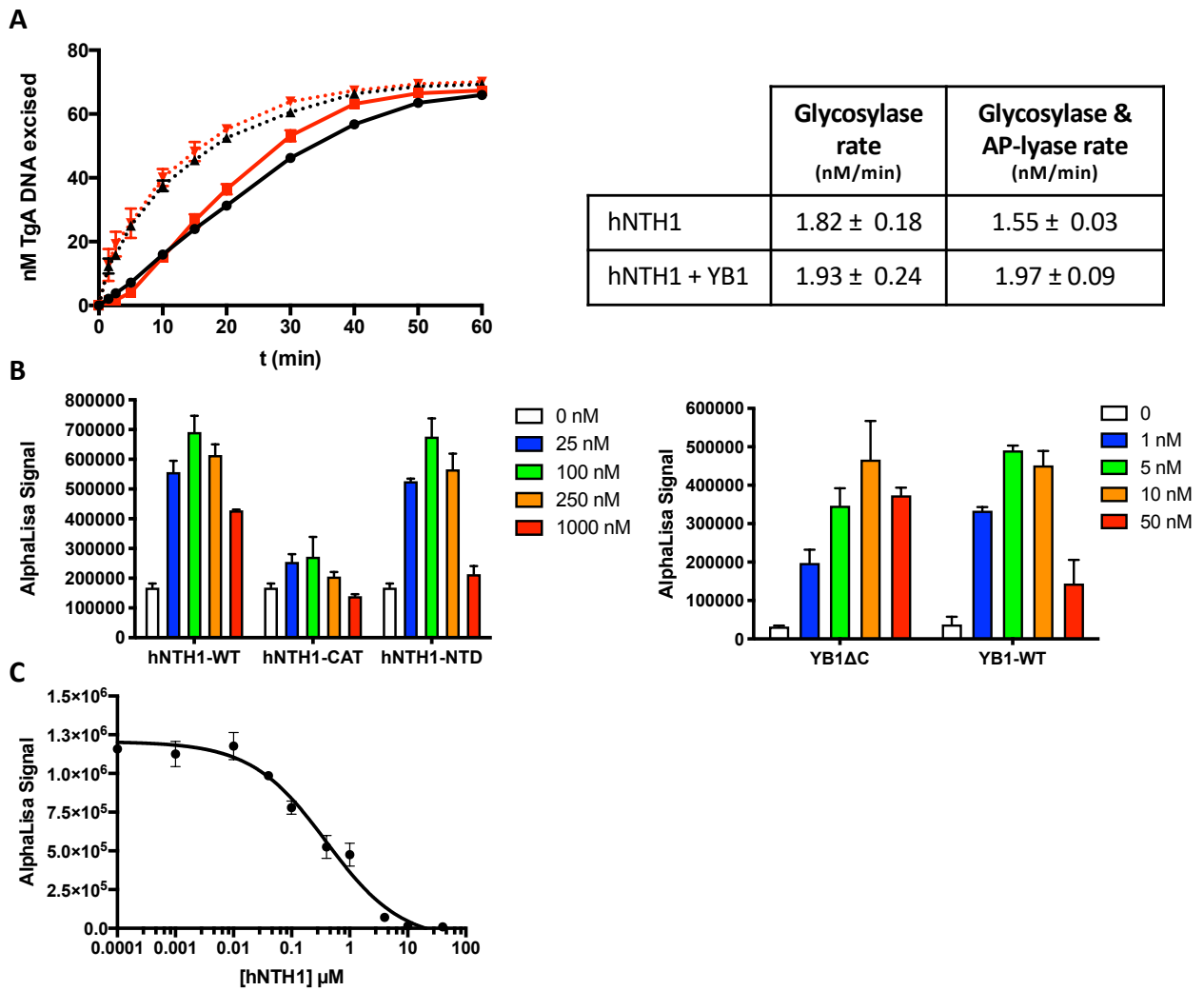


Figure 3

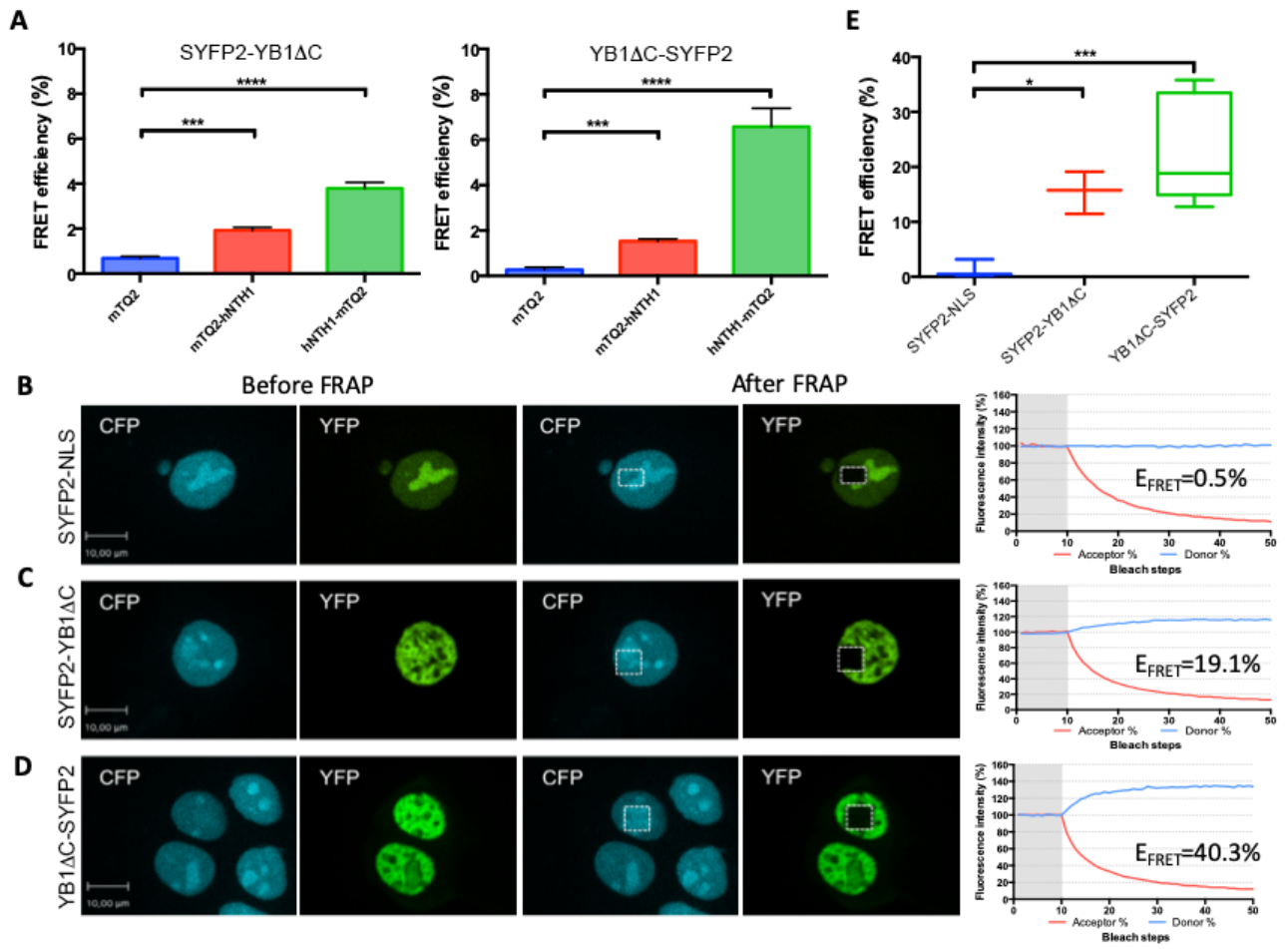


Figure 4

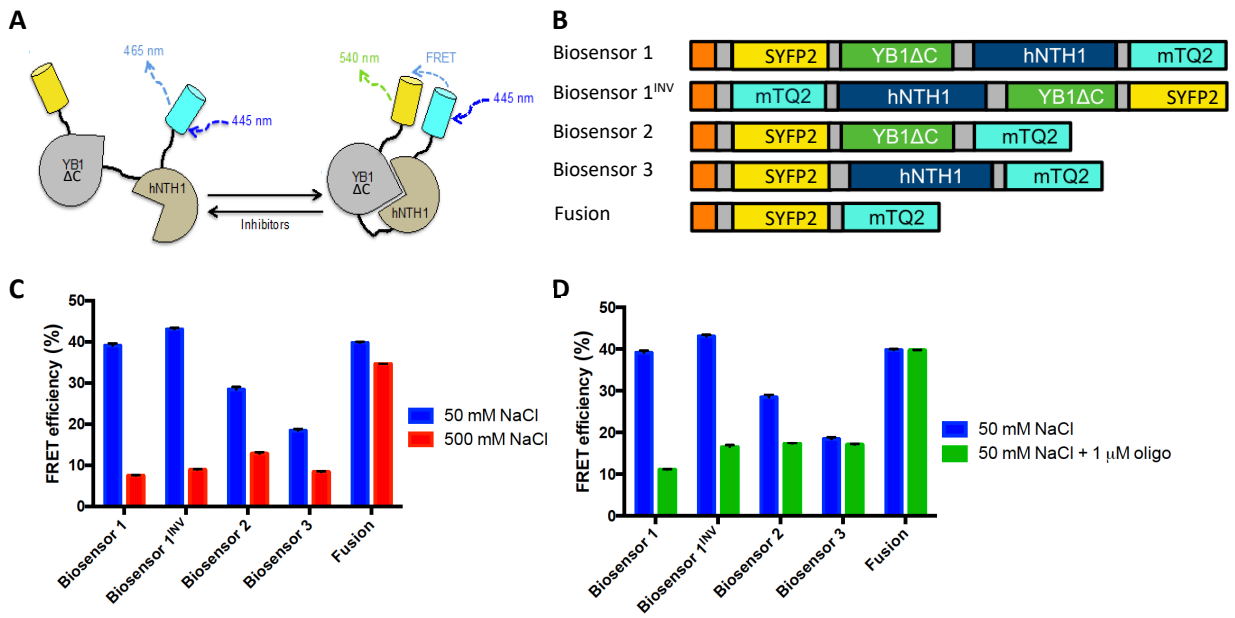


Figure 5

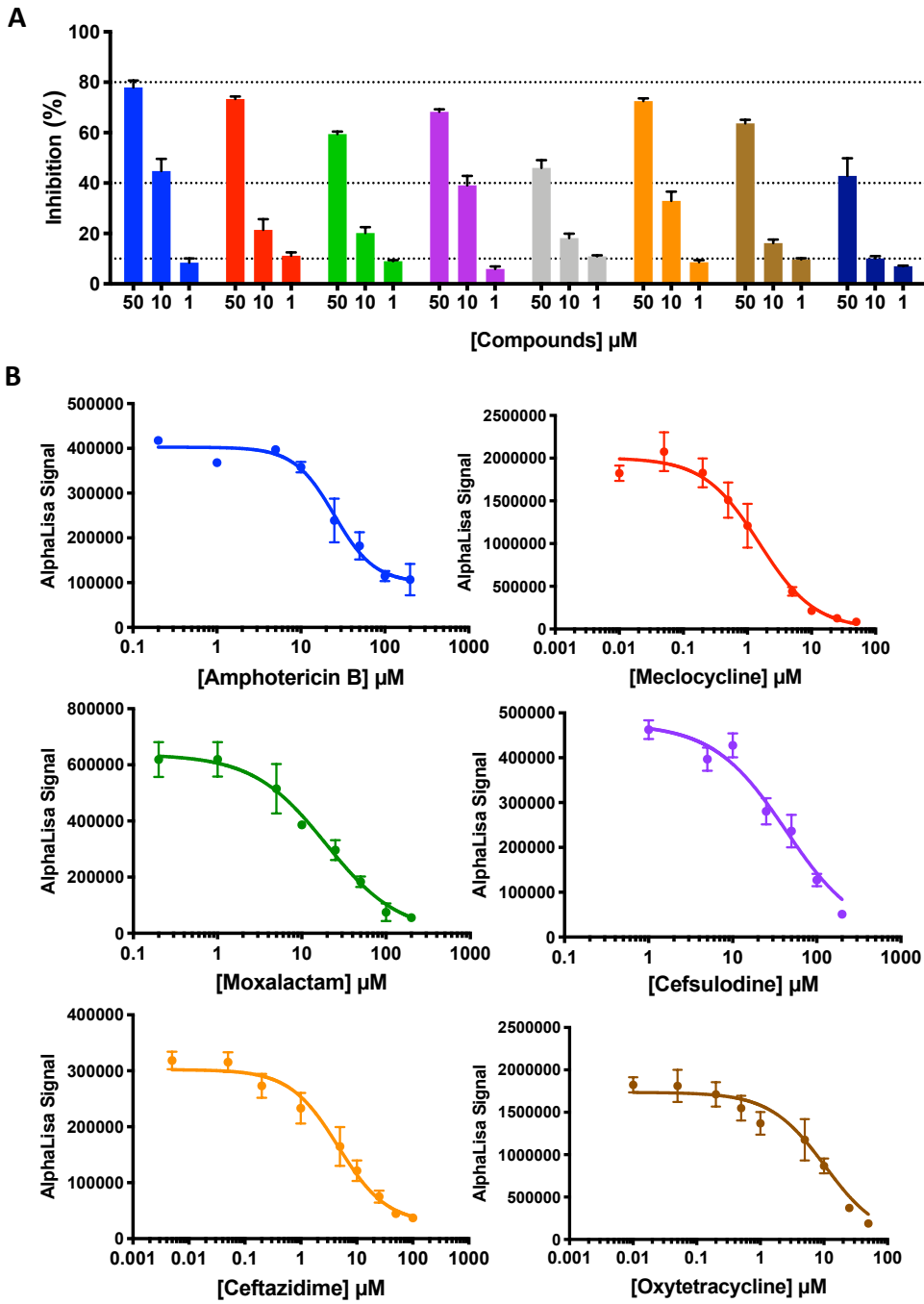


Figure 6

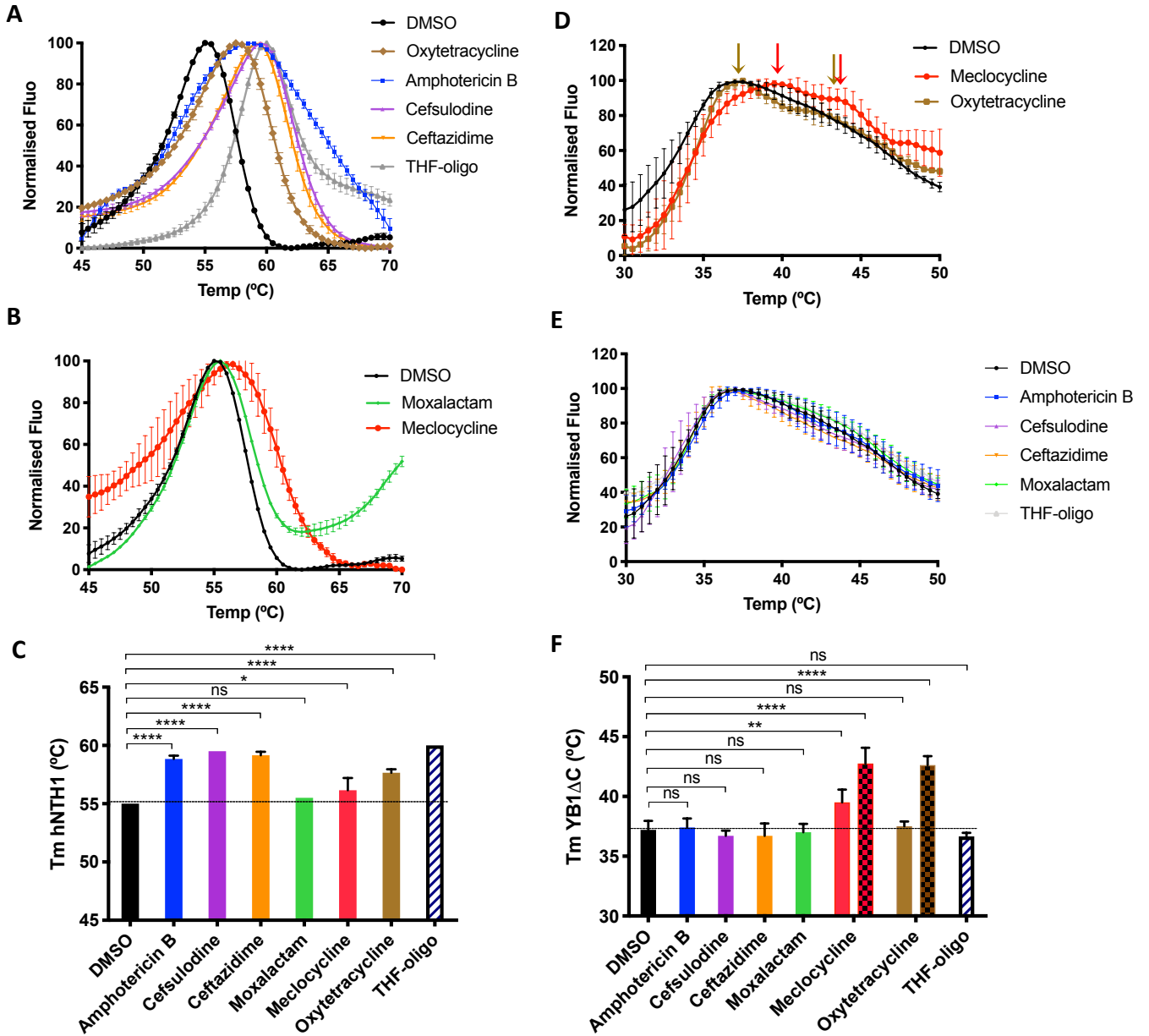
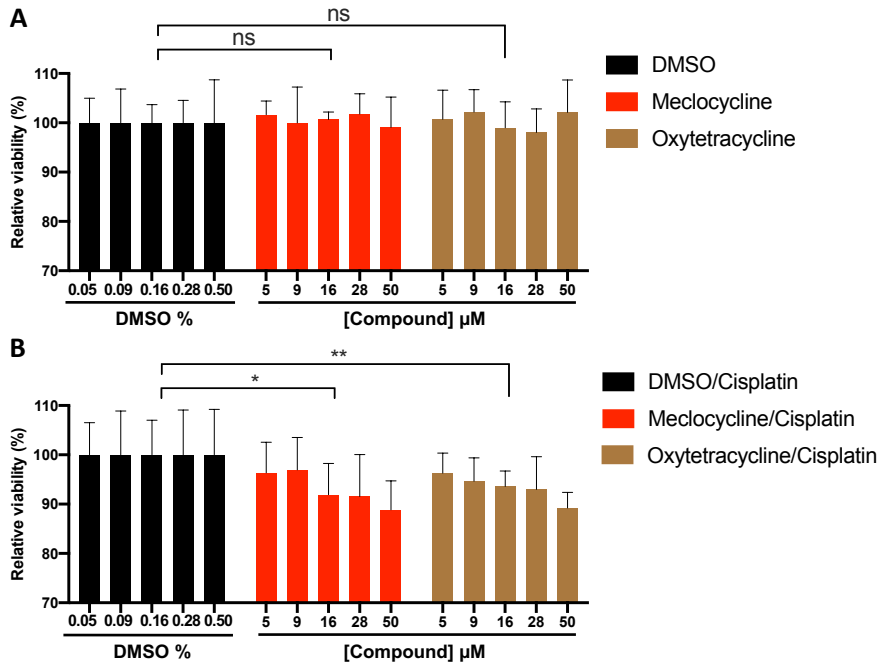


Figure 7



Förster Resonance Energy Transfer Based Biosensor for Targeting the hNTH1-YB1 Interface as a Potential Anticancer Drug Target

Muge Senarisoy¹, Caroline Barette², Françoise Lacroix¹, Salvatore De Bonis¹, Meike Stelter¹, Fabienne Hans¹, Jean-Philippe Kleman¹, Marie-Odile Fauvarque² and Joanna Timmins^{1*}.

¹Univ. Grenoble Alpes, CEA, CNRS, IBS, F-38000 Grenoble, France.

²Univ. Grenoble Alpes, CEA, INSERM, BGE, F-38000 Grenoble, France.

*Corresponding author: Joanna Timmins (Joanna.timmins@ibs.fr)

Supplemental Information

Supplemental Table S1

Supplemental Figures S1-S8

Table S1. Potential hits identified in the Prestwick Library.

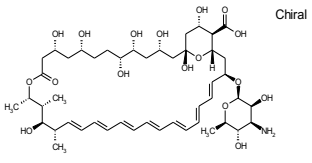
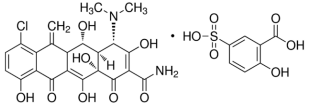
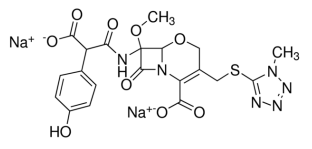
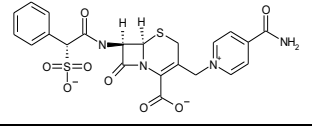
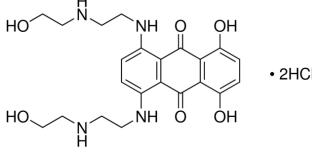
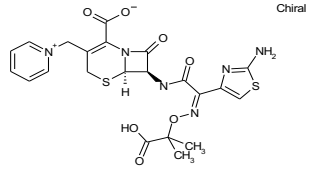
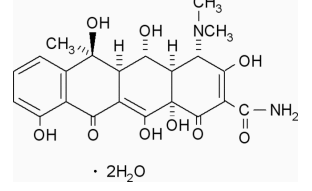
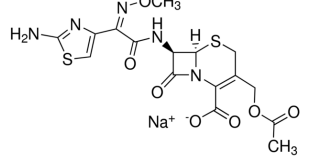
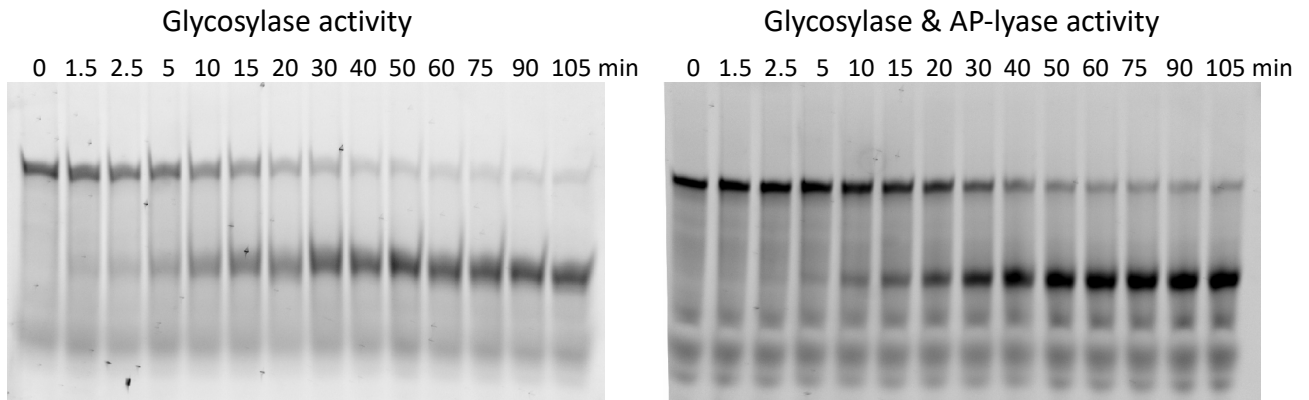
Cpd id	Chemical name	CAS no	Formula	Molecular weight (g/mol)	Inhibition (%) at 50 μ M	Molecular Structure
410	Amphotericin B	1397 - 89	$C_{47}H_{73}NO_{17}$	924	71	
456	Mecloicycline sulfosalicylate	73816 - 42	$C_{29}H_{27}ClN_2O_{14}S$	695	57	
819	Moxalactam disodium salt	64953 - 12	$C_{20}H_{18}N_6Na_2O_9S$	564	59	
814	Cefsulodine sodium salt	52152 - 93	$C_{22}H_{19}N_4NaO_8S_2$	555	66	
385	Mitoxantrone dihydrochloride	70476 - 82	$C_{22}H_{30}Cl_2N_4O_6$	517	46	
489	Ceftazidime pentahydrate	78439 - 6	$C_{22}H_{32}N_6O_{12}S_2$	637	73	
307	Oxytetracycline dihydrate	6153 - 64	$C_{22}H_{28}N_2O_{11}$	497	56	
139	Cefotaxime sodium salt	64485 - 93	$C_{16}H_{16}N_5NaO_7S_2$	478	43	

Figure S1

hNTH1



hNTH1 + YB1

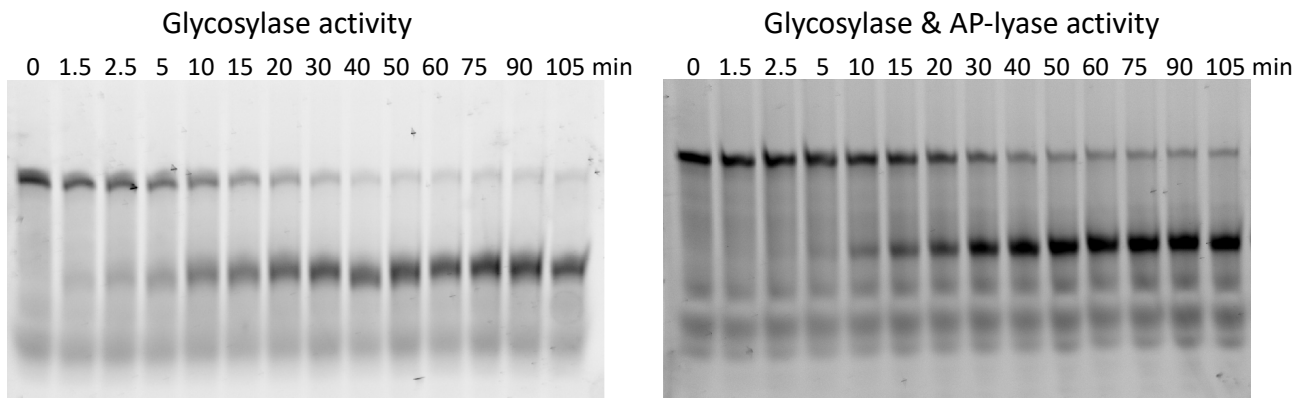


Figure S1. Examples of gels used for measuring the DNA glycosylase and AP-lyase activities of hNTH1 in the absence (upper gels) and presence of an excess of YB1 (lower gels). For the gels on the right, samples were treated with NaOH before loading them on gel, in order to cause cleavage of all strands bearing abasic sites. This allows to follow the glycosylase activity. In the gels on the left, strand cleavage was performed by the AP-lyase activity of hNTH1 following its removal of the modified base. The DNA strand containing the thymine glycol was labelled with a fluorescein moiety on the 5' end and DNA was visualized and quantified on a ChemiDoc MP Imager (Bio-Rad).

Figure S2

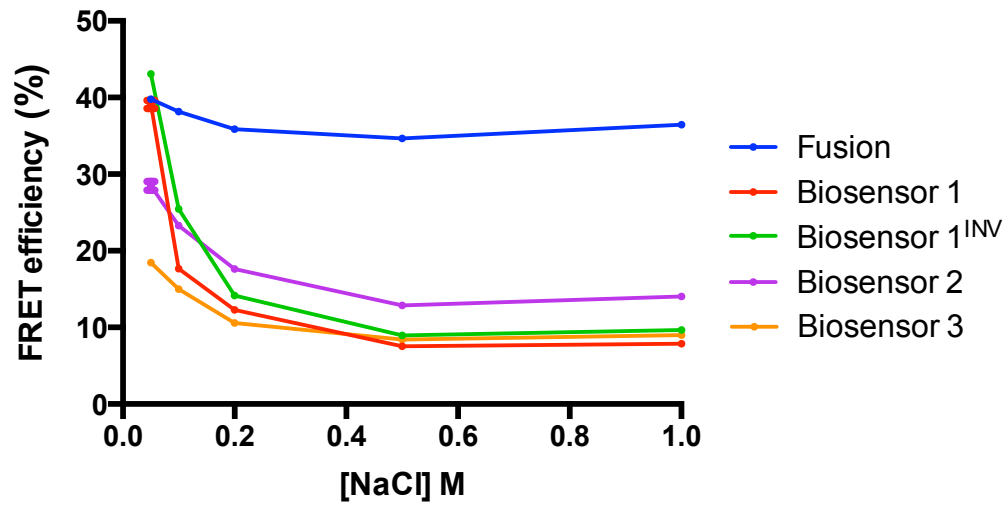


Figure S2. FRET efficiencies of 1 μ M Fusion and Biosensor constructs at different NaCl concentrations (50 mM NaCl - 1 M NaCl). The FRET signal of the Fusion is slightly affected by high salt concentrations (5% decrease). All Biosensor constructs had a basal FRET signal ranging between 8 and 15%. Biosensors 1 and 1^{INV} showed high FRET efficiencies at 50 mM NaCl, but this efficiency decreased significantly above 0.1 M NaCl, indicating that the interaction between hNTH1 and YB1 Δ C is salt-sensitive.

Figure S3

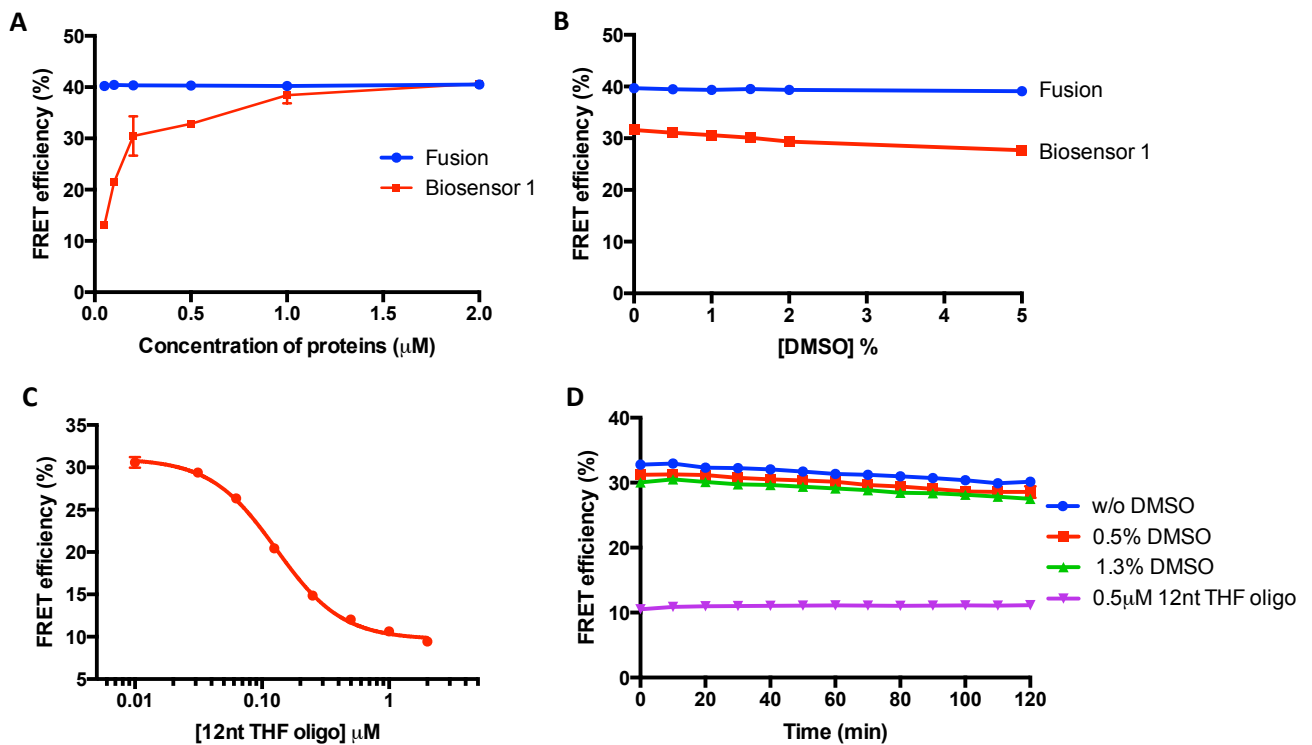


Figure S3. Optimization of Biosensor 1 as a tool for chemical library screening. (A) FRET efficiencies of Fusion and Biosensor 1 constructs at different protein concentrations in buffer containing 50 mM NaCl. The FRET signal of the Fusion was constant regardless of the protein concentration. However, the FRET signal of Biosensor 1 dropped below 0.2 μM protein concentration. Subsequent screening experiments were thus performed using 0.2 μM Biosensor 1. (B) Stability of the FRET signal of 0.2 μM Fusion and Biosensor 1 constructs in the presence of increasing amounts of DMSO (0.5, 1, 1.5, 2, and 5%). A slight decrease in the FRET efficiency of Biosensor 1 was observed at 5% DMSO. (C) Dose-dependent Inhibition of Biosensor 1 FRET by the hNTH1 DNA substrate: 12mer THF-oligo. FRET efficiencies of 0.2 μM Biosensor 1 in buffer containing 50 mM NaCl was measured in the presence of 0.01, 0.03, 0.06, 0.13, 0.25, 0.5, 1, and 2 μM THF-oligo. The data points corresponding to the means of triplicate measurements were fitted to a standard sigmoidal inhibition model in GraphPad Prism 6. (D) Stability of the FRET signal of Biosensor 1. The FRET efficiency of Biosensor 1 was monitored over a 2-hour period in buffer containing 50 mM NaCl (blue), supplemented with either 0.5% DMSO (red), 1.3% DMSO (green) or 0.5 μM THF-oligo (purple).

Figure S4

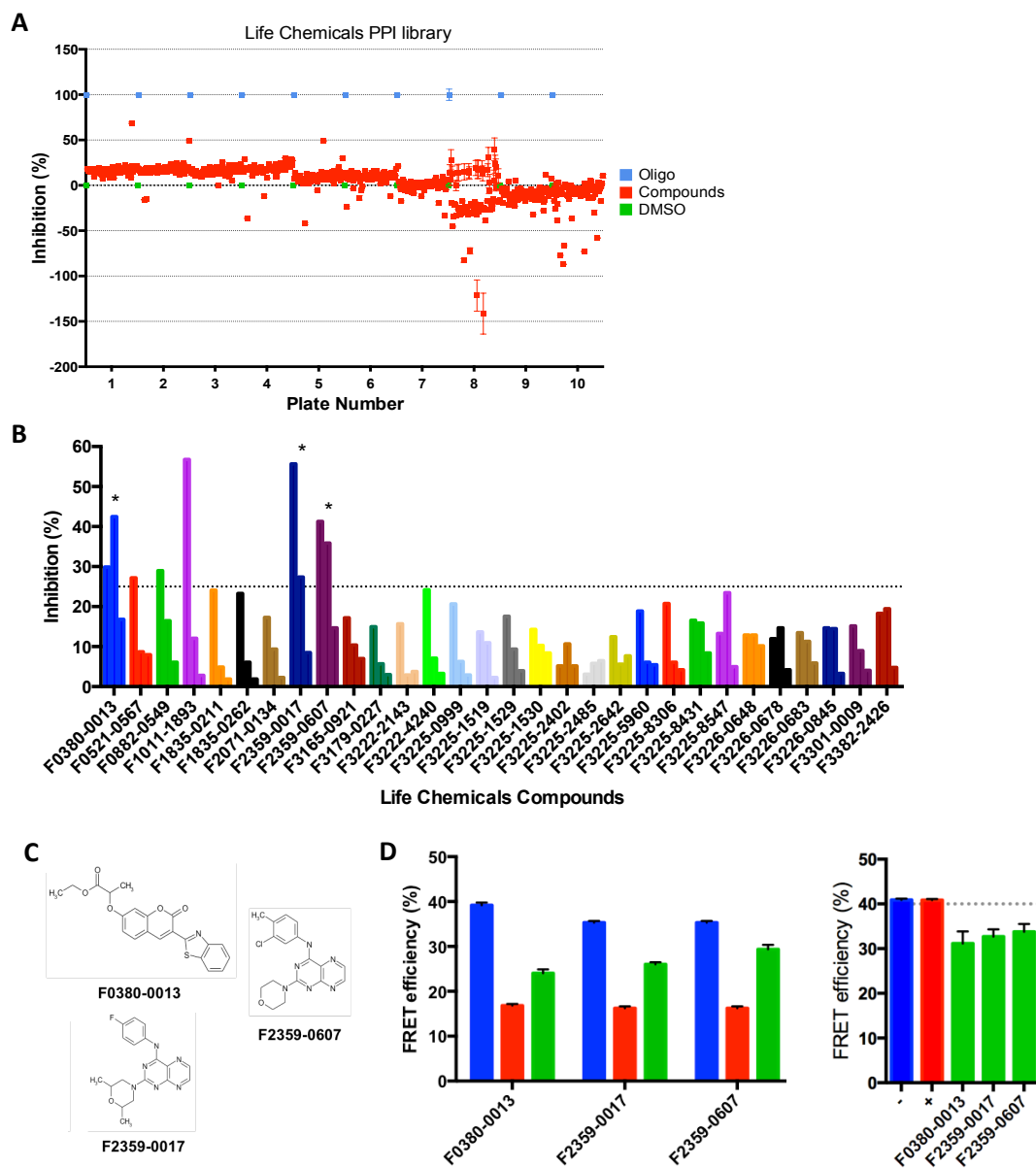


Figure S4. Results of the primary and secondary HTS of the Life Chemicals PPI fragment library and validation of the hits. (A) Overall results obtained from the primary screen. The FRET of Biosensor 1 in DMSO (green dots) was set to 0% inhibition, while the FRET of Biosensor 1 in the presence of THF-oligo (blue dots) was set to 100% inhibition. The effects of test compounds at 50 μ M from ten 384-well plates are shown as red dots in the graph. (B) Results obtained from the secondary screen of 30 selected compounds selected from the primary screen. The graph presents the extent of inhibition of Biosensor 1 FRET efficiency in the presence of these 30 compounds at 50, 10 and 1 μ M (left, middle and right histograms, respectively). The dashed line represents 25% inhibition of Biosensor 1 FRET efficiency. Selected compounds used in further validation tests are marked with an asterisk (*). (C) Chemical structures and references of the three potential hits from the Life Chemicals PPI library. (D) FRET efficiencies of 0.2 μ M Biosensor 1 (left panel) and Fusion (right panel) in the presence of either 1.3% DMSO alone (blue), 0.5 μ M THF-oligo (red) or 50 μ M compounds identified in the secondary screen (asterisk in (B); green). These initial validation experiments revealed that these were in fact false positives.

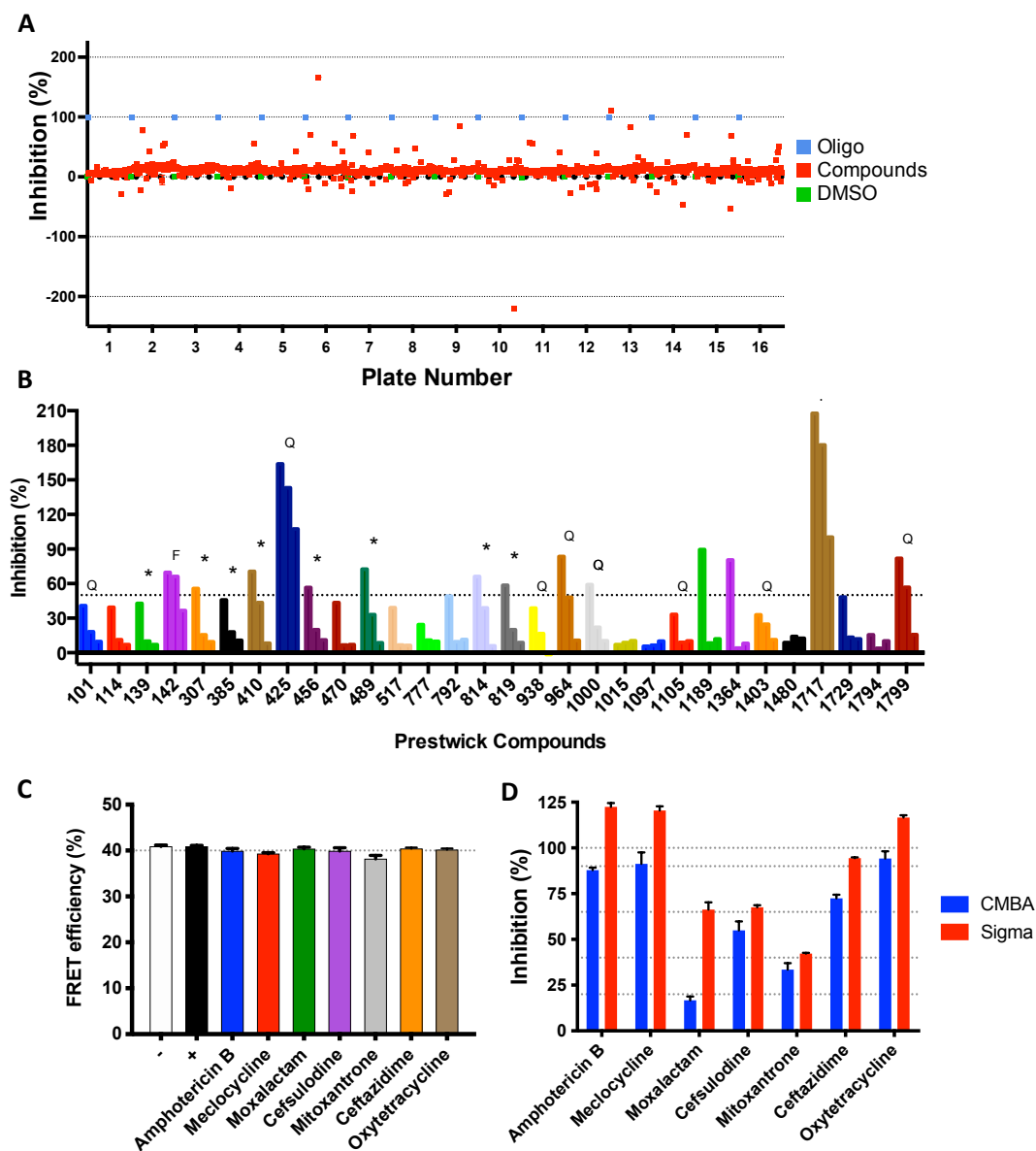
Figure S5

Figure S5. Results of the primary and secondary HTS of the Prestwick Chemical library. (A) Overall results obtained from the primary screen. The FRET of Biosensor 1 in DMSO (green dots) was set to 0% inhibition, while the FRET of Biosensor 1 in the presence of THF-oligo (blue dots) was set to 100% inhibition. The effects of test compounds at 50 μ M from sixteen 384-well plates are shown as red dots in the graph. (B) Results obtained from the secondary screen of 30 selected compounds selected from the primary screen. The graph presents the extent of inhibition of Biosensor 1 FRET efficiency in the presence of these 30 compounds at 50, 10 and 1 μ M (left, middle and right histograms, respectively). The dashed line represents 50% inhibition. Selected compounds used in further validation tests are marked with an asterisk (*). F indicates the compounds, which showed high intrinsic fluorescence signal alone. Q indicates the compounds that quenched the fluorescence signal. (C) FRET efficiencies of 0.2 μ M Fusion in buffer containing 50 mM NaCl in the presence of DMSO (blue), THF-oligo (red) or 50 μ M test compounds. No significant change was detected on the FRET signal of the Fusion construct in the presence of the seven selected Prestwick compounds. (D) Comparison of the extent of inhibition of Biosensor 1 FRET signal by seven selected Prestwick compounds either provided by the CMBA platform (blue) or prepared inhouse from powders (red).

Figure S6

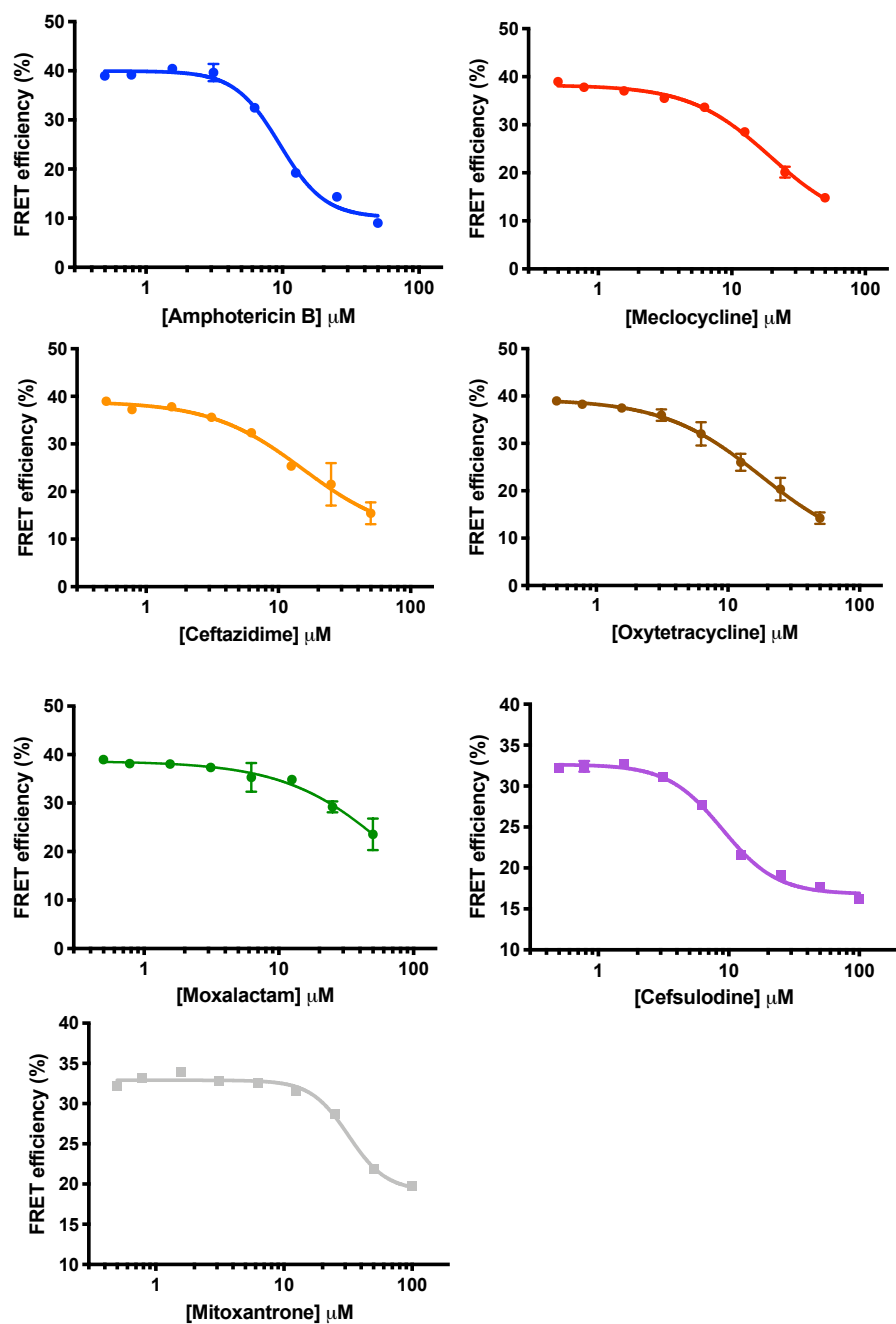


Figure S6. Dose-dependent inhibition of Biosensor 1 FRET efficiency by amphotericin B (blue), meclocycline (red), ceftazidime (orange), oxytetracycline (brown), moxalactam (green), cefsulodine (purple) and mitoxantrone (grey). The data points corresponding to the means of triplicate measurements were fitted to a 4-parameter sigmoidal inhibition model in GraphPad Prism 8 to determine the IC_{50} values (Table 1).

Figure S7

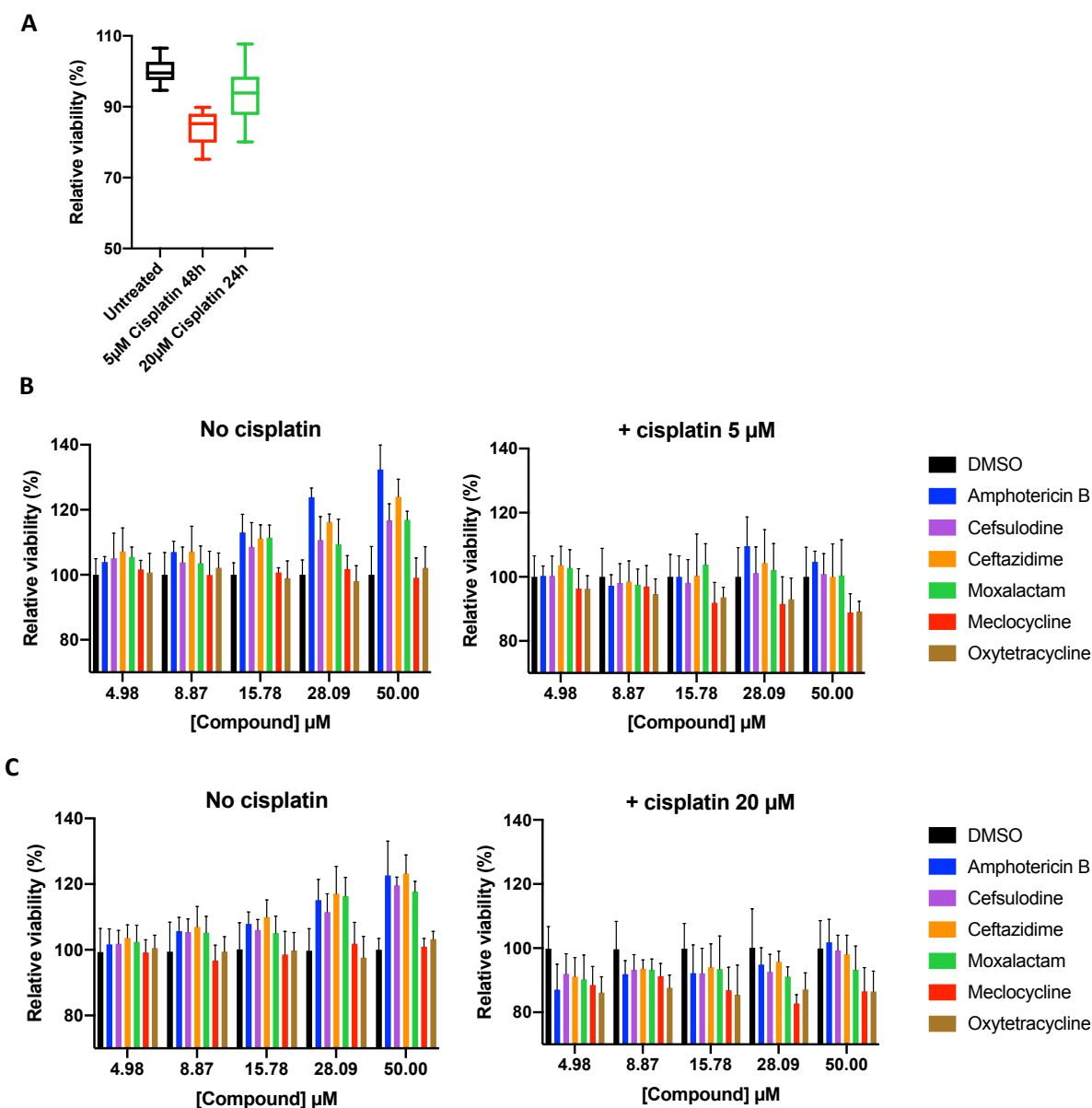


Figure S7: Effects of selected hits on the sensitivity of MCF7 cells to cisplatin. (A) Effects of cisplatin on MCF7 viability. The relative viability of MCF7 cells treated with either 5 or 20 µM cisplatin for respectively 48 and 24 h was compared to that of untreated cells. The box-and-whiskers plot presents the median, min. and max. of 20 replicates. (B) Relative viability of MCF7 cells treated with either 5-50 µM selected compounds or DMSO (black) only (left panel) or with both 5-50 µM selected compounds or DMSO (black) and 5 µM cisplatin for 48 h (right panel). Plotted histograms are the mean of four replicates and error bars represent the standard deviation. (C) Relative viability of MCF7 cells treated with either 5-50 µM selected compounds or DMSO (black) only (left panel) or with both 5-50 µM selected compounds or DMSO (black) and 20 µM cisplatin for 24 h (right panel). Plotted histograms are the mean of four replicates and error bars represent the standard deviation. (A)-(C) The viability of DMSO treated cells at each concentration was set to 100% and was used as a reference for calculating the relative viability of cisplatin and/or compound-treated cells. All graphs were prepared with GraphPad Prism 8.

Figure S8

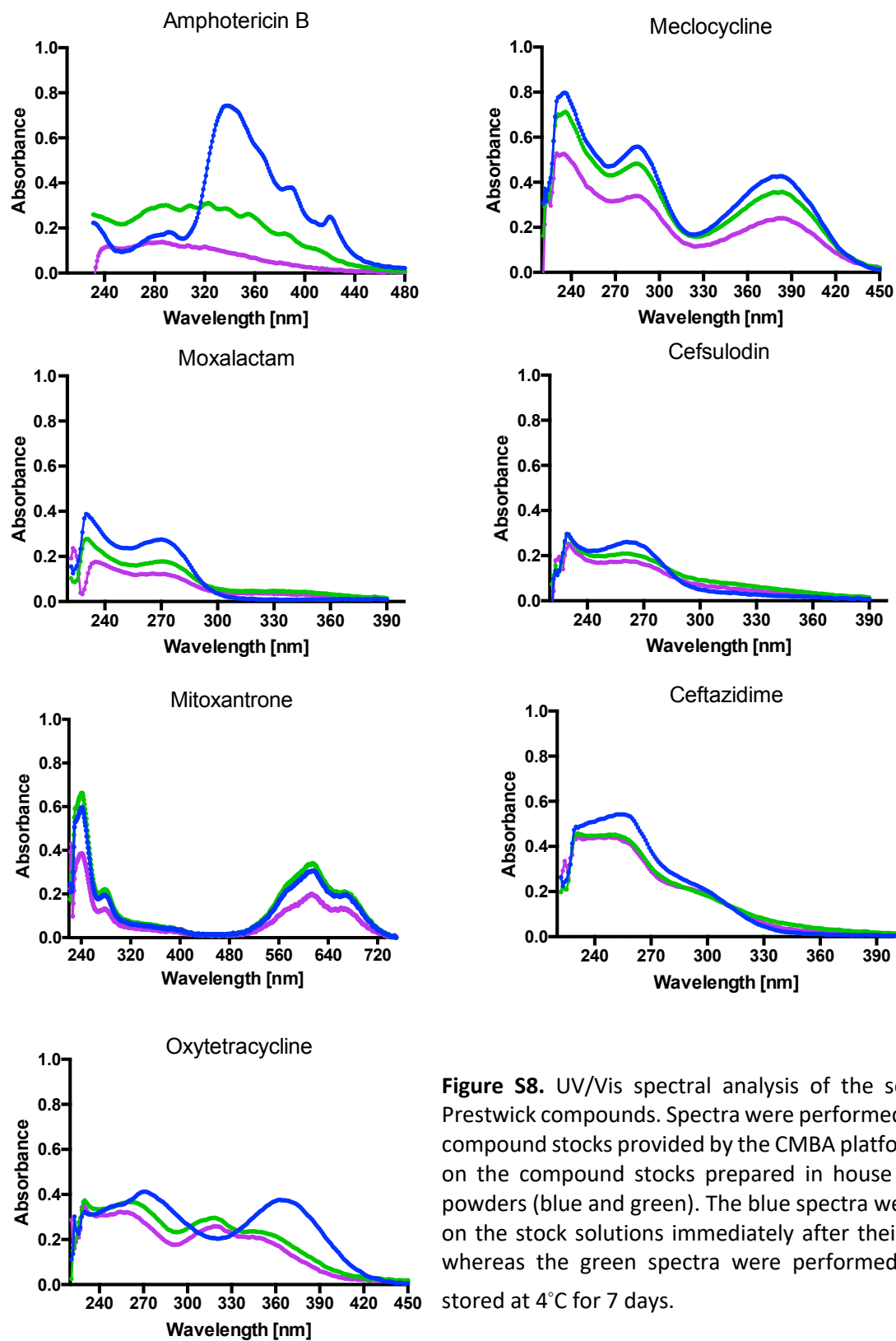


Figure S8. UV/Vis spectral analysis of the seven selected Prestwick compounds. Spectra were performed either on the compound stocks provided by the CMBA platform (purple) or on the compound stocks prepared in house starting from powders (blue and green). The blue spectra were performed on the stock solutions immediately after their preparation, whereas the green spectra were performed on solutions stored at 4°C for 7 days.